TISSUE ENGINEERING: Part C
Volume 17, Number 2, 2011
© Mary Ann Liebert, Inc.
DOI: 10.1089/ten.tec.2010.0139

Transplantation of Human Adipose Tissue-Derived Multilineage Progenitor Cells Reduces Serum Cholesterol in Hyperlipidemic Watanabe Rabbits

Hanayuki Okura, Ph.D.,[1,2] Ayami Saga, M.S.,[1] Yuichi Fumimoto, M.D., Ph.D.,[1] Mayumi Soeda, V.M.D.,[1] Mariko Moriyama, Ph.D.,[1,3] Hiroyuki Moriyama, Ph.D.,[3] Koji Nagai, M.D.,[1,4] Chun-Man Lee, M.D., Ph.D.,[1] Shizuya Yamashita, M.D., Ph.D.,[5] Akihiro Ichinose, M.D., Ph.D.,[4] Takao Hayakawa, Ph.D.,[3] and Akifumi Matsuyama, M.D., Ph.D.[1]

Familial hypercholesterolemia (FH) is an autosomal codominant disease characterized by high concentrations of proatherogenic lipoproteins and premature atherosclerosis secondary to low-density lipoprotein (LDL) receptor deficiency. We examined a novel cell therapy strategy for the treatment of FH in the Watanabe heritable hyperlipidemic (WHHL) rabbit, an animal model for homozygous FH. We delivered human adipose tissue-derived multilineage progenitor cells (hADMPCs) via portal vein and followed by immunosuppressive regimen to avoid xenogenic rejection. Transplantation of hADMPCs resulted in significant reductions in total cholesterol, and the reductions were observed within 4 weeks and maintained for 12 weeks. ^{125}I-LDL turnover study showed that the rate of LDL clearance was significantly higher in the WHHL rabbits with transplanted hADMPCs than those without transplanted. After transplantation hADMPCs were localized in the portal triad, subsequently integrated into the hepatic parenchyma. The integrated cells expressed human albumin, human alpha-1-antitrypsin, human Factor IX, human LDL receptors, and human bile salt export pump, indicating that the transplanted hADMPCs resided, survived, and showed hepatocytic differentiation *in vivo* and lowered serum cholesterol in the WHHL rabbits. These results suggested that hADMPC transplantation could correct the metabolic defects and be a novel therapy for inherited liver diseases.

Introduction

Familial hypercholesterolemia (FH) is characterized by premature and accelerated development of atherosclerotic lesions caused by elevated levels of cholesterol-rich lipoproteins in plasma. The disease is caused by mutations in the low-density lipoprotein (LDL) receptor gene that result in a significant decrease in receptor-mediated uptake of lipoproteins from the circulation.[1–3] Patients homozygous for defects in LDL receptors have serum cholesterol levels 5–10 times those of normal and suffer as early as the first two decades of life from complications such as coronary artery disease.[4,5] In homozygous FH patients, conventional drug therapy cannot treat the condition, and therapeutic recourses are limited to chronic plasmapheresis or orthotopic liver transplantation.[1] Although liver transplants lower LDL levels, the procedure is life threatening; in addition, donor livers are in short supply. Cellular transplantation has been proposed to provide functional LDL receptors for the treatment of hypercholesterolemia. Transplantation of allogenic and xenogenic hepatocytes has been shown to be effective in lowering serum cholesterol in the Watanabe heritable hyperlipidemic (WHHL) rabbit,[6–9] which is an animal model for homozygous FH. Further, a number of gene therapy approaches have shown some promises in animal models and human,[10–13] and the therapies will cure a number of patients with FH in near future. As an alternative to whole-organ transplantation and/or gene therapy, we have investigated the ability of human adipose tissue-derived multilineage progenitor cells (hADMPCs) to differentiate into hepatocytes *in vitro* and to replace critical liver functions[14] as well as previous reports,[15,16] because the *in vitro* differentiation of hADMPCs into various kinds of cell types in now well reported and hADMPCs can be easily and safely obtained in large

[1]Department of Somatic Stem Cell Therapy and Health Policy, Foundation for Biomedical Research and Innovation, Kobe, Japan.
[2]Research Fellow of the Japan Society for the Promotion of Science, Tokyo, Japan.
[3]Pharmaceutical Research and Technology Institute, Kinki University, Osaka, Japan.
[4]Department of Plastic Surgery, Kobe University Hospital, Kobe, Japan.
[5]Division of Cardiology, Department of Internal Medicine, Osaka University Graduate School of Medicine, Osaka Japan.

quantities without serious ethics issues.[17,18] In this study, we are investigating whether hADMPCs could differentiate into hepatocytes *in vivo* and replace critical liver functions as considerable therapeutic potential for cellular replacement.

Materials and Methods

Cells

hADMPCs were prepared as described previously[19] with some modifications.[14,17,18] Adipose tissues from human subjects were resected during plastic surgery in five subjects (four males and one female, age, 20–60 years) as excess discards. Ten to 50 g of subcutaneous adipose tissue was collected from each subject. All subjects provided informed consent. The protocol was approved by the Review Board for Human Research of Kobe University Graduate School of Medicine, Osaka University Graduate School of Medicine, and Foundation for Biomedical Research and Innovation. After five to six passages, the hADMPCs were used for transplantation. Human cryopreserved hepatocytes were purchased from Invitrogen (Lot number: HuP81) and cultured as indicated by the manufacturer's protocol. Human adipose tissue-derived fibroblastic cells were obtained according to previous report.[20]

Flow cytometric analysis

hADMPCs isolated from adipose tissue were characterized by flow cytometry. Cells were detached from culture dishes by 0.25% trypsin/ethylenediaminetetraacetic acid (EDTA) and suspended in Dulbecco's phosphate-buffered saline (DPBS; Nacalai Tesque) containing 0.1% fetal bovine serum. Aliquots (5×10^5 cells) were incubated for 30 min at 4°C with fluorescein isothiocyanate-conjugated mouse monoclonal antibodies to human CD31 (BD PharMingen), CD105 (Ancell Corporation), CD133 (R&D Systems), phycoerythrin-conjugated mouse monoclonal antibodies to human CD29, CD34, CD45, CD73 (BD PharMingen), CD44, or CD166 (Ancell). Isotype-identical antibodies served as controls. Further, the cells were incubated with mouse monoclonal antibodies against human stage-specific embryonic antigen-4 (from Chemicon International, Inc.), ABCG-2, or CD117 (BD PharMingen) with nonspecific mouse antibody used as a negative control. After washing with DPBS, cells were incubated with phycoerythrin-labeled goat anti-mouse Ig antibody (BD PharMingen) for 30 min at 4°C. After three washes, cells were resuspended in DPBS and analyzed by flow cytometry using a FACSCalibur flow cytometer and CellQuest Pro software (BD Biosciences).

Adipogenic, osteogenic, and chondrogenic differentiation procedure

For adipogenic differentiation, cells were cultured in the differentiation medium (Zen-Bio, Inc.). After 3 days, half of the medium was changed with adipocyte medium (Zen-Bio) every 2 days. Five days after differentiation, adipocytes were characterized by microscopic observation of intracellular lipid droplets by Oil Red O staining. Osteogenic differentiation was induced by culturing the cells in Dulbecco's modified Eagle's medium containing 10 nM dexamethasone, 50 mg/dL ascorbic acid 2-phosphate, 10 mM β-glycerophosphate (Sigma), and 10% fetal bovine serum. Differentiation was examined by Alizarin red staining. For Alizarin red staining, the cells were washed three times and fixed with dehydrated ethanol. After fixation, the cells were stained with 1% Alizarin red S in 0.1% NH_4OH (pH 6.5) for 5 min and then washed with H_2O. For chondrogenic differentiation, hADMPCs were first trypsinized and 2×10^5 cells were centrifuged at 400 *g* for 10 min. The resulting pellets were cultured in the chondrogenic medium (alpha-minimum essential medium (alpha-MEM) supplemented with 10 ng/mL transforming growth factor-β, 10 nM dexamethasone, 100 μM ascorbate, and 10 μL/mL 100×ITS Solution) for 14 days. For Alcian Blue staining, nuclear counterstaining with Weigert's hematoxylin was followed by 0.5% Alcian Blue 8GX for proteoglycan-rich cartilage matrix.

hADMPC transplantation and immunosuppression regimen

WHHL rabbits (8 weeks old; purchased from Kitayamalabes, Inc.) were anesthetized with pentobarbital (50 mg/kg). An incision distal and parallel to the lower end of the ribcage was made. The peritoneum was incised, and hADMPCs ($n=5$) or human adipose tissue-derived fibroblastic cells ($n=3$) (3×10^7 cells) suspended in 3 mL of Hanks' balanced salt solutions (HBSS) (20°C) or 3 mL of control saline ($n=6$) were infused in 5 min into the portal vein via a 18-gauge Angiocath™ (BD). The immunosuppression regimen (Fig. 1A) consisted of the following: (1) intramuscular injection of cyclosporin A (6 mg/kg/day) daily from the day before surgery to sacrifice; (2) intramuscular injection of rapamycin (0.05 mg/kg/day) daily from the day before surgery to sacrifice; (3) methylprednisolone at 3 mg/kg/day (days 1–7), followed by tapering to 2 mg/kg/day (days 8–14), 1 mg/kg/day (days 15–21) and 0.5 mg/kg/day (day 22 to the time at sacrifice); (4) intravenous injection of cyclophosphamide (20 mg/kg/day) at days 0, 2, 5, and 7; (5) ganciclovir (2.5 mg/kg/day intramuscular injection (i.m.)) was also administrated to avoid viral infection in the immunocompromised host.

DNA extraction and quantification of human-derived cells

Total DNA of WHHL rabbit liver, which was obtained at the time just after hADMPC transplantation, and 2, 4, 8, and 12 weeks after transplantation, were isolated using a NucleoSpin Tissue kit (Macherey-Nagel) according to the manufacturer's instructions. hADMPCs and rabbit hepatocytes were mixed at the ratios of 100:0 (100%), 10:90 (10%), 1:99 (1%), 0.1:99.9 (0.1%), 0.01:99.99 (0.01%), and 0.001:99.999 (0.001%), and DNA was isolated. Seven hundred nanograms of each samples of extracted DNA was quantified by real-time polymerase chain reaction (PCR) using the ABI Prism 7900 Sequence Detection System (Applied Biosystems), primers for the 82 bp *Alu* amplicon (forward, 5′-GTCAGGAGATCGA GACCATCCC; reverse, 5′-CCACTACGCCCGGCTAATTT), and SYBR Green (TOYOBO) dye using a previously published protocol.[21,22] Reactions were performed in quadruplicate and the *Alu* levels were calculated by the standard curve.

Assay for lipid profiling

Serum samples were obtained from nonfasting rabbits before and after transplantation. Serum total cholesterol was measured in each sample using assay kits from Wako Pure Chemical Industries. Serum lipoproteins were analyzed by an on-line dual enzymatic method for simultaneous quantification of cholesterol and triglycerides by high-performance

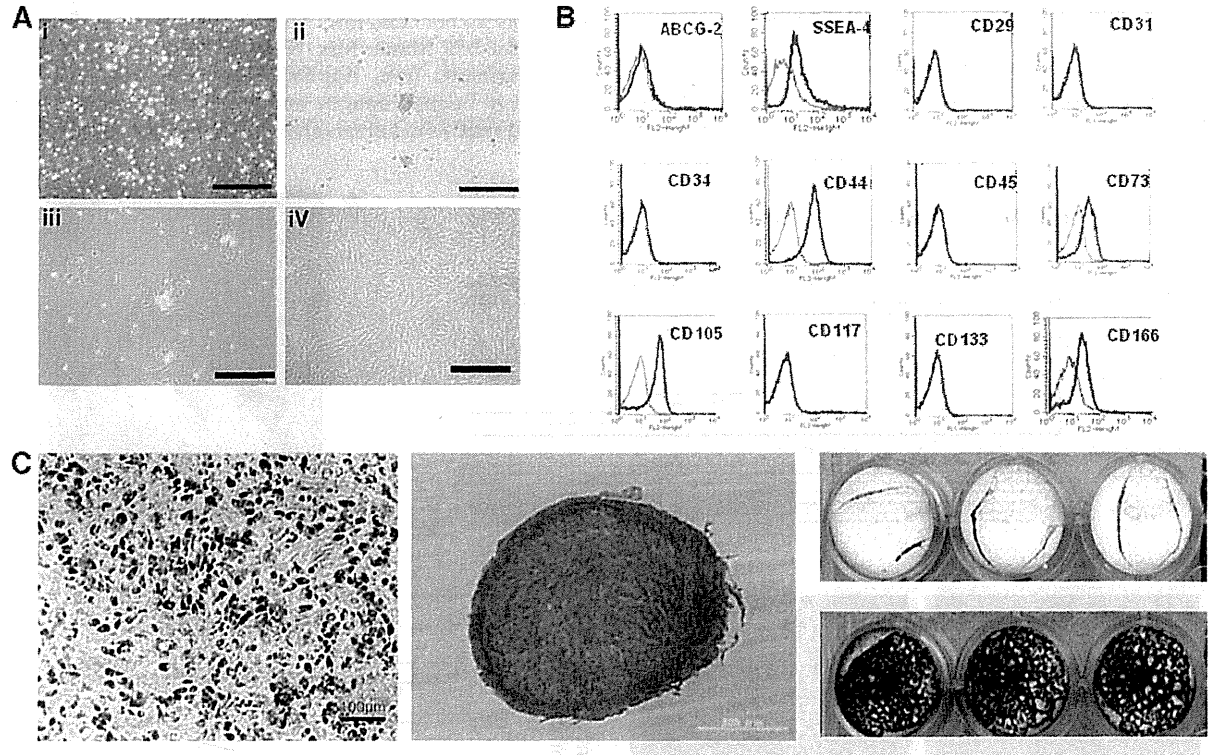

FIG. 1. **(A)** Morphological characters of human adipose tissue-derived multilineage progenitor cells (hADMPCs). The cells obtained from adipose tissue were seeded and incubated for 24 h **(i)**. After incubation, the adherent cells were treated with ethylenediaminetetraacetic acid solution, and the resulting suspended cells were replated at a density of 10,000 cells/cm^2 on human fibronectin-coated dishes (BD BioCoat) **(ii, iii)**. Within two to three passages after the initial plating of the primary culture, hADMPCs appeared as a monolayer of large flat cells (25–30 μm in diameter). As the cells approached confluence, they assumed a more spindle-shaped, fibroblastic morphology **(iv)**. i) Bar = 499 μm, ii) bar = 201 μm, iii) bar = 502 μm and iv) bar = 202 μm. **(B)** Cell surface markers expressed on hADMPCs. The cells were negative for markers of the hematopoietic lineage (CD45) and of hematopoietic stem cells, ABCG-2, CD34, and CD133. They were also negative for CD31, an endothelial cell-associated marker, and the surface antigen c-Kit (CD117). However, they stained positively for a number of surface markers characteristic of mesenchymal and/or neural stem cells, but not embryonic stem (ES) cells, including CD29, CD44 (hyaluronan receptor), CD73, CD105 (endoglin), and CD166. hADMPCs also were positive for stage-specific embryonic antigen (SSEA)-4. **(C)** Adipocytic, chondrocytic, and osteocytic differentiation potentials of hADMPCs. Adipocytic differentiation potential of hADMPCs was confirmed by Oil Red O staining (the left panel) (bar = 100 μm). Chondrocytic differentiation potential of hADMPCs was estimated by extracellular matrices with Alcian Blue staining (the middle panel). Osteogenic differentiation potential of hADMPCs was confirmed by Alizarin red S staining for mineralized nodules (the right panel).

liquid chromatography at Skylight Biotech, according to the procedure as described.[23]

Immunohistochemical staining of WHHL rabbit liver sections

The WHHL livers were harvested and fixed immediately with 10% formalin. They were placed into optimal cutting temperature compound (Sakura Finetechnical Co.), frozen immediately, and then sectioned at 7 μm thickness. The sections were then incubated with blocking solution (Blocking one; Nacalai Tesque) for 1 h. The samples were incubated with rabbit anti-human-specific albumin antibody (MBL), rabbit anti-human-specific alpha 1 anti-trypsin antibody, and rabbit anti-LDL receptor antibody, followed by Alexa Fluor 488-labeled goat anti-rabbit IgG (Molecular Probes). To show the colocalization of human CD90 and albumin, the samples were incubated with the rabbit anti-human CD90 monoclonal antibody (Epitomics, Inc.) and then with Alexa Fluor 488-labeled goat anti-rabbit IgG (Molecular Probes), and washed extensively. Then, the specimens were incubated with rabbit anti-human-specific albumin antibody (MBL), followed by Alexa Fluor 546-labeled goat anti-rabbit IgG (Molecular Probes). The treated sample was examined with a BioZero laser scanning microscope (Keyence).

PCR analysis of WHHL rabbit liver for human liver-specific genes

Total RNAs of WHHL rabbit liver, hADMPCs, and human hepatocytes were isolated using an RNAeasy kit (Qiagen). After treatment with DNase, the cDNA was synthesized using Superscript III RNase H-minus Reverse Transcriptase (Invitrogen). Real-time PCR was performed using the ABI Prism 7900 Sequence Detection System (Applied Biosystems). About 20×Assays-on-Demand™ Gene Expression Assay Mix for human alpha-1-antitrypsin (Hs01097800_m1), human albumin (Hs00609411_m1), human factor 9, human GATA-binding

protein 4 (GATA4) (Hs00171403_m1), human hepatocyte nuclear factor 3 beta (Hs00232764_m1), human LDL receptor (Hs00181192_m1), and human glyceraldehyde-3-phosphate dehydrogenase (Hs99999905_m1) were obtained from Applied Biosystems. It was confirmed that human detectors and rabbit detectors do not cross-react with the other species. TaqMan® Universal PCR Master Mix, No AmpErase® UNG (2×), was also purchased from Applied Biosystems. Reactions were performed in quadruplicate and the mRNA levels were normalized relative to human glyceraldehyde-3-phosphate dehy-

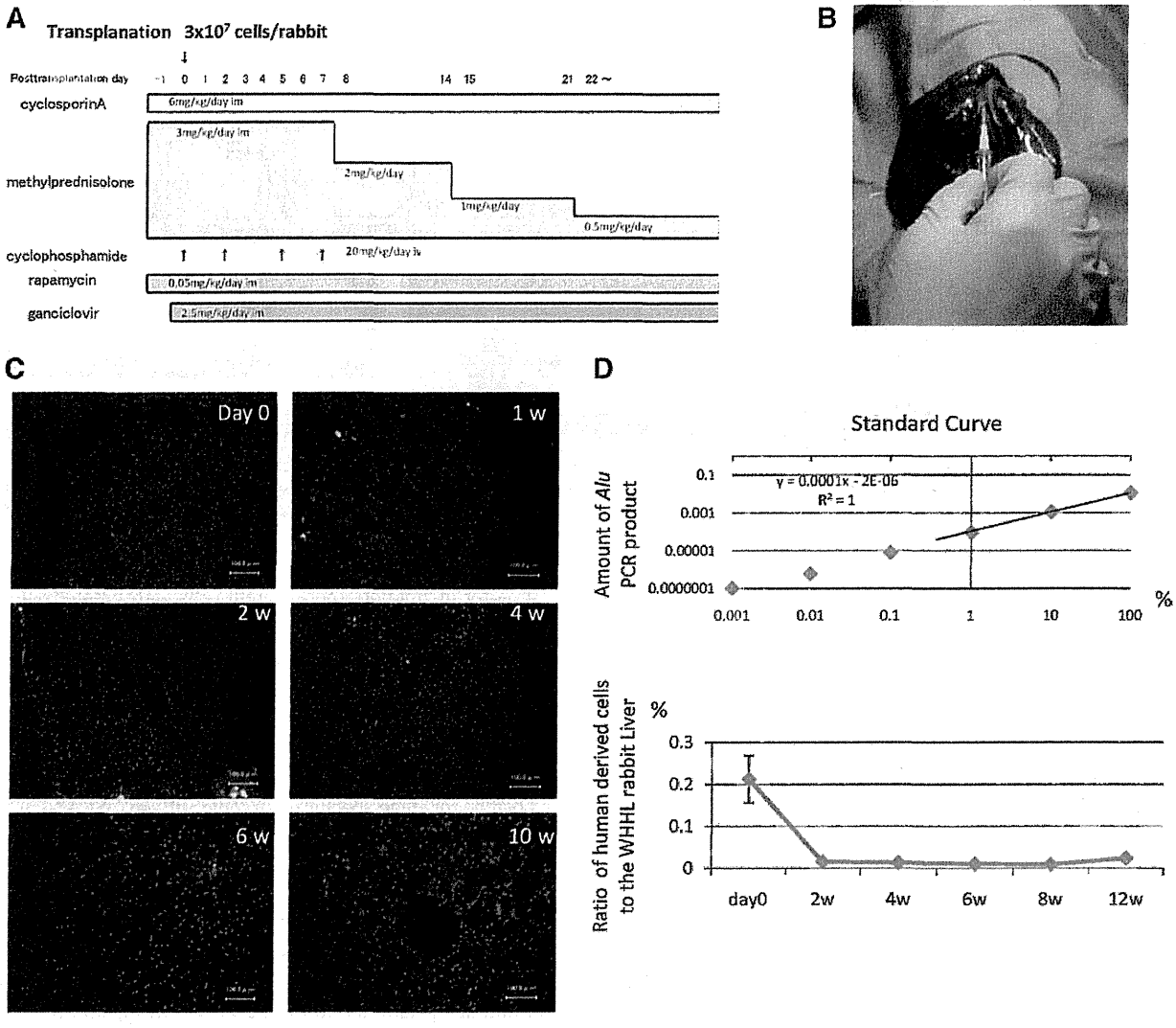

FIG. 2. **(A)** Immunosuppression regimen. Cyclosporin A (6 mg/kg/day) and rapamycin (0.05 mg/kg/day) were administered intramuscularly daily from the day before surgery to sacrifice. Methylprednisolone was administered at 3 mg/kg/day (days 1–7), 2 mg/kg/day (days 8–14), 1 mg/kg/day (days 15–21), and 0.5 mg/kg/day (day 22 to sacrifice). Cyclophosphamide (20 mg/kg/day) was injected intravenously at days 0, 2, 5, and 7. Ganciclovir (2.5 mg/kg/day) was also injected intramuscularly to avoid viral infection in the immunocompromised host. **(B)** Surgical procedure. Watanabe heritable hyperlipidemic (WHHL) rabbits were anesthetized with pentobarbital. An incision was made distal and parallel to the lower end of the ribcage. The peritoneum was incised and hADMPCs, and human adipose tissue-derived fibroblastic cells (hADFCs) (3×10^7 cells/rabbit) or controls were infused into the portal vein using an 18-gauge Angiocath. **(C)** Localization of transplanted hADMPCs in the WHHL liver. At the day of and 1, 2, 4, 6, and 10 weeks after transplantation of DiI-labeled hADMPCs via the portal vein, the WHHL rabbit liver was examined histologically. DiI-fluorescent labeled-hADMPCs resided and distributed in the portal area at the day of transplantation. One to 2 weeks after transplantation, the DiI-stained hADMPCs-derived cells were localized near the portal areas. Four weeks after transplantation some of the DiI-stained cells resembled innate hepatocytes morphologically. Six and 10 weeks after transplantation, DiI-positive transplanted cells were dispersed in a centrilobular direction, resembling the mature innate hepatocytes. Bars = 100 μm. **(D)** Quantification of repopulation of the transplanted cells in the liver. The ratios of human-derived cell repopulation were examined by analyzing an *Alu* repetitive DNA sequence at the day of and 2, 4, 8, and 12 weeks after transplantation. In upper panel the standard curve was indicated, and in lower panel the ratio of repopulation of human cells was shown in time course after transplantation of hADMPCs.

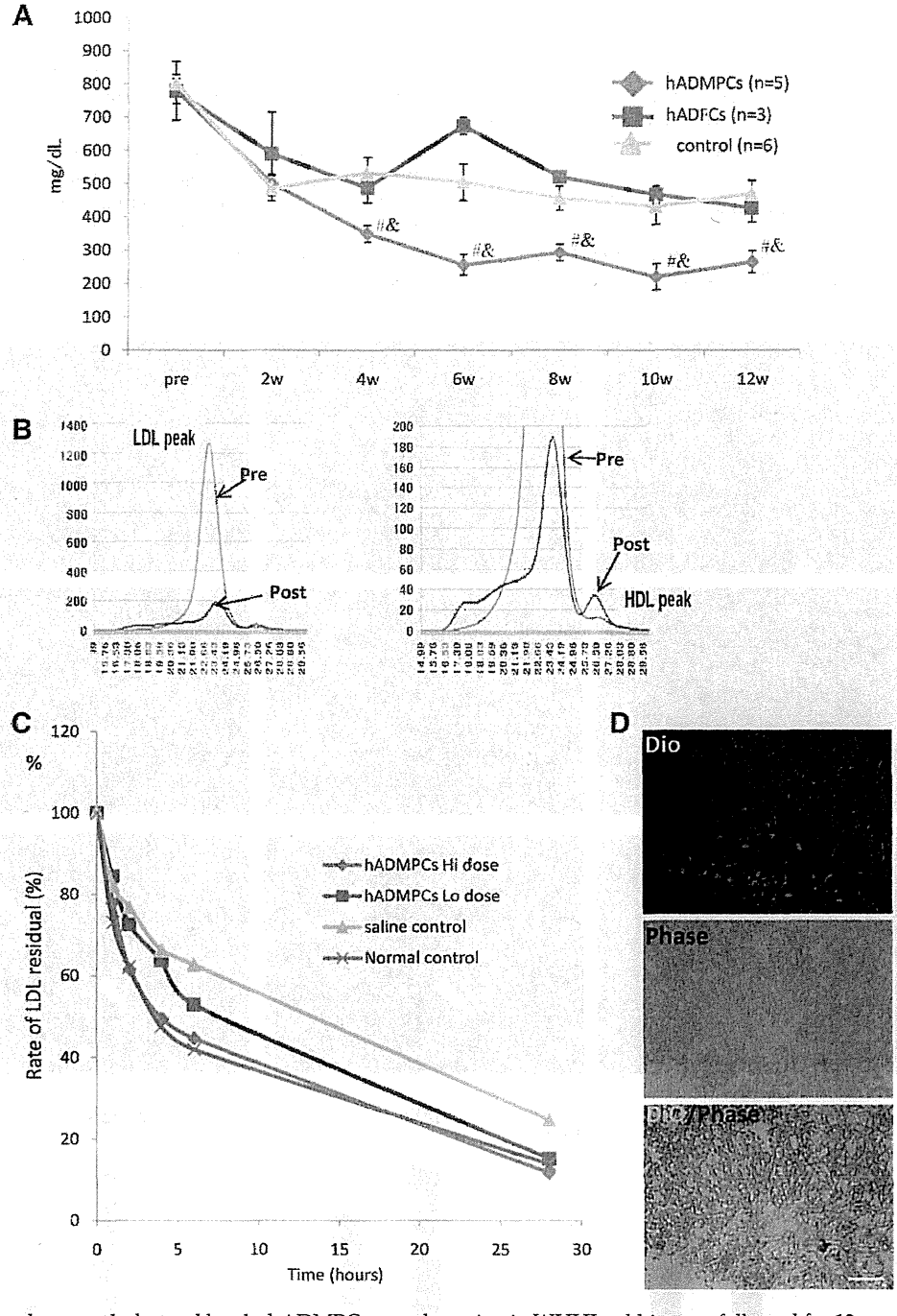

FIG. 3. **(A)** Total serum cholesterol levels. hADMPC transplantation in WHHL rabbits was followed for 12 weeks. Total serum cholesterol was measured in five rabbits that each received 3×10^7 hADMPCs, three rabbits that each received 3×10^7 hADFCs, and in six rabbits that received saline (control). Bars indicated mean ± standard error of the mean (SEM) ($^{\#}p < 0.05$; control vs. the hADMPC-transplanted WHHL rabbit; $^{\&}p < 0.05$; the hADFC-transplanted WHHL rabbit vs. the hADMPC-transplanted WHHL rabbit). **(B)** Lipoprotein profiles in a representative WHHL rabbit with hADMPC transplantation after gel filtration. Serum samples from the WHHL rabbit before and 4 weeks after transplantation were fractionated. Note the marked reduction in low-density lipoprotein (LDL) peak and appearance of high-density lipoprotein (HDL) peak. **(C)** Rate of clearance of LDL from the serum of rabbits with and without transplantation of hADMPCs. Animals were injected with ^{125}I-labeled human LDL, and the time course of clearance was monitored following trichroloacetic acid precipitation of serum at time 5 min, 1 h, 2 h, 4 h, 6 h, and 28 h. Residual ^{125}I-LDL was expressed as percentages of that at 5 min. $^{\#}p < 0.05$ (control vs. the hADMPC-transplanted WHHL rabbit [low dose]) and $^{*}p < 0.05$ (control vs. the hADMPC-transplanted WHHL rabbit [high dose]). **(D)** DiO-LDL uptake into hADMPC-derived hepatocytes in the WHHL rabbi liver. Thin-sliced recipient liver was incubated with DiO-labeled LDL in the serum-free medium for 24 h. After washing and fixation, the incubated slices were applied for fluorescent microscopy. DiO-LDL uptake cells (green) and no uptake parenchymal cells were observed in the section. Bar = 100 μm.

drogenase expression. To confirm that hADMPCs differentiated into hepatocytes *in vivo*, the cells before transplantation and human primary hepatocytes (Invitrogen, Lot number; HuP81) were applied for quantitative PCR as control.

Clearance of ^{125}I-LDL from rabbit serum

WHHL rabbits (8 weeks old) were anesthetized with pentobarbital (50 mg/kg). The peritoneum was incised and hADMPCs (high-dose; 3×10^7 cells/rabbit, $n=2$, low-dose; 5×10^6 cells/rabbit, $n=2$) suspended in 3 mL of HBSS (20°C) ($n=5$) or 3 mL of control saline ($n=2$) were infused into the portal vein via a 18-gauge Angiocath (BD). The rabbits were immunosuppressed using the protocol illustrated in Figure 1A. Eight weeks later, the animals were tested by the LDL turnover assay. ^{125}I human LDL (BT-913R, Lot No. 9130709; Biomedical Technologies Inc.) was delivered via the marginal ear vein of the WHHL rabbits and normal control

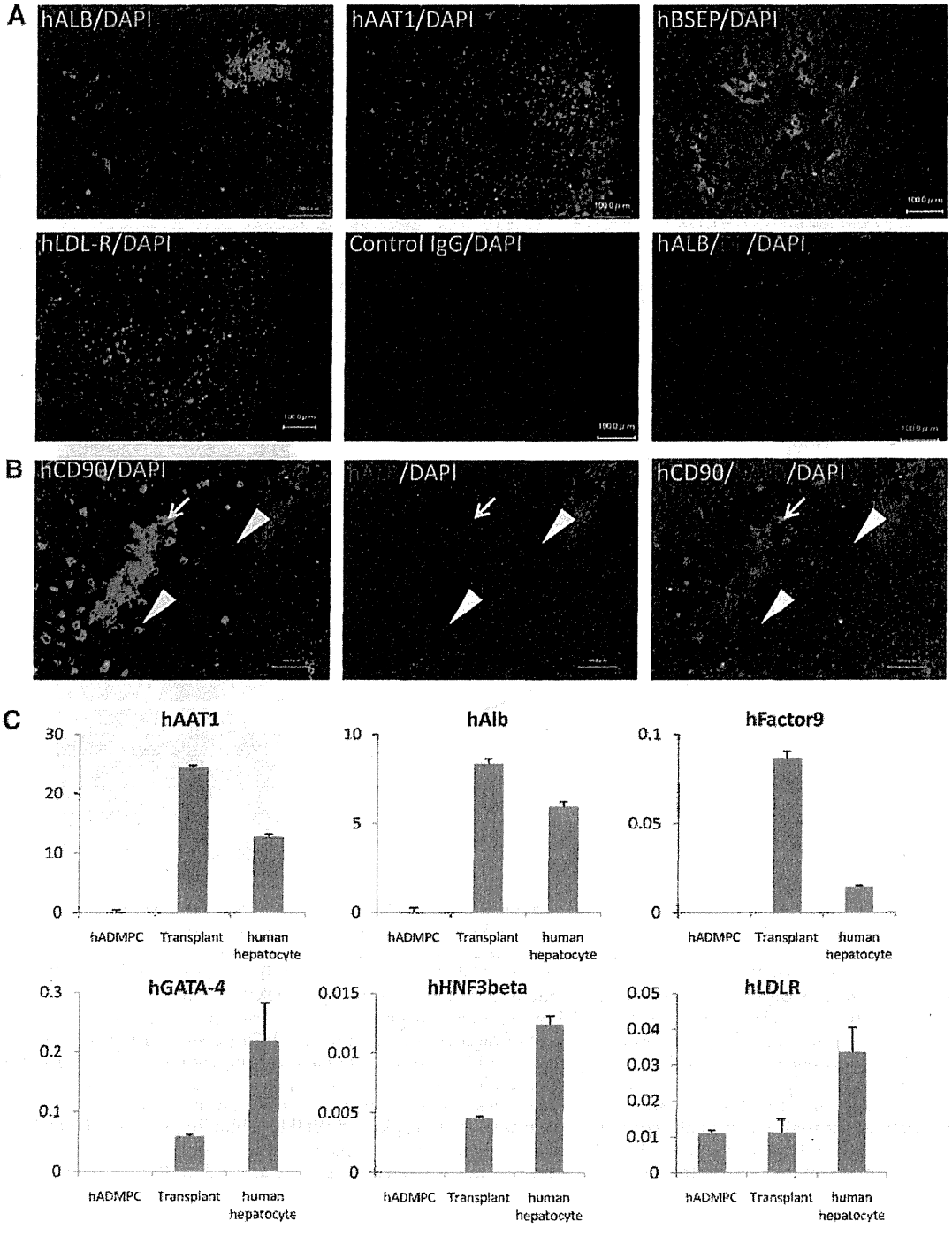

rabbits in physiological saline containing 2 mg/mL bovine serum albumin. Blood was collected from the opposite ear after injection at 5 min, 1 h, 2 h, 4 h, 6 h, and 28 h. ^{125}I-labeled apolipoprotein B-containing LDL was precipitated with 20% of trichloroacetic acid (Wako Pure Chemical Industries) (serum; 320 μL, 100% w/v trichloroacetic acid (TCA) 80 μL), and then the precipitants were applied for counting.

Uptake of DiO-labeled LDL by transplants ex vivo

Human LDL (1.019–1.063 g/mL) was isolated by sequential ultracentrifugation from normolipidemic donors as previously described,[24] dialyzed against saline-EDTA, and then sterilized by filtration through a 0.2 μm filter. Lipoproteins were labeled with 3,3′-dioctadecyloxacarbocyanine perchlorate (DiO; Sigma) by incubating the LDL in 0.5% bovine serum albumin/PBS with 100 mL DiO in dimethyl sulfoxide (3 mg/mL) for 8 h at 37°C. The lipoproteins were obtained by sequential ultra centrifugation (1.019–1.063 g/mL) as described,[14] and then dialyzed against PBS and filtered before use. To evaluate the uptake of DiO-LDL by transplants *ex vivo*, thin-sliced WHHL rabbit liver tissue were incubated with serum-free Dulbecco's modified Eagle's medium containing 10 μg/mL DiO-LDL for 24 h at 37°C. Finally, the incubated slices were rinsed, fixed with 10% formalin, sectioned into 5 μm thickness, and mounted with Perma-Flour (Japan Tanner Corporation). The slides were examined using a BioZero laser scanning microscope (Kyence).

Statistical analysis

Values were expressed as mean ± standard error of the mean. Differences between mean values of treated and untreated groups were evaluated using the Student's *t*-test. A p-value < 0.05 was considered statistically significant. All statistical analyses were performed using the SPSS Statistics 17.0 package (SPSS Inc.).

Results

Characteristics of hADMPCs

The cells obtained from adipose tissue were seeded and incubated for 24 h (Fig. 1Ai). After incubation, the adherent cells were treated with EDTA solution, and the resulting suspended cells were replated at a density of 10,000 cells/cm^2 on human fibronectin-coated dishes (BD BioCoat) (Fig. 1Aii and 1Aiii). Within two to three passages after the initial plating of the primary culture, hADMPCs appeared as a monolayer of large flat cells (25–30 μm in diameter). As the cells approached confluence, they assumed a more spindle-shaped, fibroblastic morphology (Fig. 1Aiv). After passaging five to six times, the hADMPCs were applied for transplantation. We used flow cytometry to assess markers expressed by hADMPCs (Fig. 1B). The cells were negative for markers of the hematopoietic lineage (CD45) and of hematopoietic stem cells, ABCG-2, CD34, and CD133. They were also negative for CD31, an endothelial cell-associated marker and the surface antigen c-Kit (CD117). However, they stained positively for a number of surface markers characteristic of mesenchymal and/or neural stem cells, but not embryonic stem cells, including CD29, CD44 (hyaluronan receptor), CD73, CD105 (endoglin), and CD166. hADMPCs also were positive for stage-specific embryonic antigen-4. Next, adipogenic, osteogenic, and chondrogenic differentiation potential of hADMPCs were examined (Fig. 1C). Adipogenic differentiation was induced by culture with differentiation medium containing 1-methyl-3-isobutylxanthine (a peroxisome proliferator-activated receptor γ agonist), dexamethasone, and insulin. Induction was confirmed by the accumulation of intracellular lipid droplets that were stained with Oil Red O. After 7-day induction for osteogenesis, hADMPCs were stained with Alizarin red S for mineralized nodules. hADMPCs showed intense Alcian Blue staining, indicating chondrogenic induction capability of hADMPCs.

Serum cholesterol in WHHL rabbit with transplants

hADMPCs were separated from human subcutaneous adipose tissues, cultured for five to seven passages, and applied for transplantation into WHHL rabbits. WHHL rabbits received immunosuppressants and an antiviral agent as illustrated in Figure 2A, and then were transplanted 3×10^7 hADMPCs by portal vein infusion (Fig. 2B). At the day of and 1, 2, 4, 6, and 10 weeks after transplantation of hADMPCs via the portal vein, we examined whether the cells reside or not in the liver after transplantation. Typical

FIG. 4. **(A)** Immunohistochemical identification of human hepatocytic marker cells in liver sections of WHHL rabbits after hADMPC transplantation. Twelve weeks after hADMPC transplantation, human albumin-, human alpha-1-antitrypsin-, human bile salt export pump (BSEP)-, and LDL-receptor-positive cells were dispersed within the perivenous regions of the liver parenchyma, where they made contact with and integrated among the host cells with cell–cell interactions between hADMPC-derived cells and diseased hepatocytes pair. Ten weeks after transplantation of DiI-stained hADMPCs, copresence of human albumin (green) and pretreated DiI-fluorescence (red) on the same cells was observed. Bar = 100 μm. **(B)** Differentiation of transplanted hADMPCs into hepatocyte-like cells. Twelve weeks after transplantation, almost but not all human CD90-positive cells expressed human albumin, indicating that major population of transplanted hADMPCs could differentiate into hepatocyte-like cells (left panel: human CD90; middle panel: human albumin; right panel: merge). Arrows indicate human CD90 and human albumin double-positive cells; arrowheads indicate human CD90-positive but human albumin-negative cells. **(C)** Human hepatic gene expression in WHHL rabbit liver after hADMPC transplantation. RNA was prepared from the WHHL rabbit liver 12 weeks after hADMPC transplantation. We used the following hepatic markers: human alpha-1-antitrypsin, human albumin, human factor IX, human GATA-binding protein 4 (GATA-4), human hepatocyte nuclear factor 3 (HNF-3) beta, and human LDL-receptor. Their expression levels were examined by quantitative real time-polymerase chain reaction (RT-PCR) using Assays-on-Demand Gene Expression Assay Mix. The livers of WHHL rabbits that received saline ($n = 3$) were negative for human hepatic genes. The mRNA levels were normalized based on human glyceraldehyde-3-phosphate dehydrogenase expression as housekeeping gene and data are mean ± SEM of triplicate experiments. The livers of WHHL rabbits that received hADMPC transplantation ($n = 3$) were positive for human hepatic genes, and their expression levels were similar to those of human primary hepatocytes but not hADMPCs *per se*. Data are mean ± SEM.

distribution patterns of transplanted hADMPCs were followed in Figure 2C. DiI-fluorescent labeled-hADMPCs resided and distributed in the portal area at the day of transplantation. Six and 10 weeks after transplantation, DiI-positive transplanted cells migrated into centrilobular direction. Next, to demonstrate certain percentage of repopulation of the transplanted cells in the liver, the ratios of human-derived cell repopulation were examined by analyzing a repetitive DNA sequence at the day of and 2, 4, 6, and 12 weeks after transplantation (Fig. 2D). To indicate standard curve, we mixed the indicated percentage of hADMPCs with rabbit hepatocytes and plotted the obtained the amount of *Alu* PCR products, and estimated the amount of repopulation of the transplanted cells in the liver. At the day of transplantation, the ratio of hADMPCs to whole WHHL rabbit liver cells was $0.21\% \pm 0.056\%$ (mean ± standard error of the mean) and the ratio decreased to $0.016\% \pm 0.002\%$, $0.011\% \pm 0.001\%$, and $0.009\% \pm 0.0001\%$ after 2, 4, and 8 weeks of transplantation, respectively. After 12 weeks of transplantation, the ratio was increased to $0.024\% \pm 0.00005\%$ as indicated (Fig. 2D).

To reveal the effects of hADMPC transplantation onto the lipid profiles of the WHHL rabbit, serum cholesterol levels were monitored over 12 weeks (Fig. 3A). Significant reductions in total serum cholesterol were observed within 4 weeks of the transplantation, and the reductions were maintained for the entire period. The reduction in serum cholesterol in the animals that received hADMPC transplantation was significantly greater than that of the control group. To determine the effects of hADMPC transplantation on the fractions of high-density lipoprotein and LDL in recipient animals, fractionation by fast protein liquid chromatography was performed (Fig. 3B). Transplantation of hADMPCs resulted in marked reduction of the peak LDL-cholesterol and increment of high-density lipoprotein cholesterol fraction (right panel).

Next, clearance experiments were performed with human LDL to confirm that the transplanted hADMPCs contributed the fall in serum cholesterol through uptake of LDL via LDL receptors. The rate of LDL clearance was significantly higher in the WHHL rabbits with transplanted hADMPCs than WHHL rabbits without transplanted hADMPCs (Fig. 3C). Rabbits with hADMPC transplants showed ~2.4-fold (high-dose; 3×10^7 cells/rabbit) and 1.4-fold (low-dose; 5×10^6 cells/rabbit) increase in the rate of LDL cholesterol clearance.

To evaluate the uptake of DiO-LDL by transplants *ex vivo*, thin-sliced WHHL rabbit liver was incubated with DiO-labeled LDL for 24 h and the uptake was examined as clearance experiment (Fig. 3D). DiO-LDL was uptaken by some but not all of the cells in the WHHL rabbit liver transplanted with hADMPCs. The DiO-LDL-uptaking cells were seen dispersed, contacted, and integrated among the nonuptaking parenchymal cells, suggesting that hADMPCs differentiated into hepatocytes *in vivo*, lowered of serum cholesterol via LDL uptake.

hADMPCs reside, survive, and differentiate into hepatocytes in vivo

After establishment of the graft as indicated by long-term lowering of serum cholesterol, human-specific hepatocytic proteins, such as albumin, alpha-1-antitrypsin, bile salt export pump, and LDL-receptor, positive cells were identified dispersed within perivenous regions of the liver parenchyma, where they have contacted and integrated among the host cells (Fig. 4A), with cell–cell interactions conserved between hADMPC-derived hepatocytes and diseased hepatocytes pair. Ten weeks after transplantation of DiI-prestained hADMPCs, copresence of human albumin (green) and pretreated DiI-fluorescence (red) on the same cells was observed (Fig. 4A), indicating the transplanted hADMPCs might differentiate into hepatocyte-like cells. To confirm transplanted hADMPCs might differentiate into hepatocyte-like cells and to reveal the efficacy of differentiation, the colocalization of human CD90 and human albumin was examined. As shown in Figure 4B, almost but not all human CD90-positive cells expressed human albumin, indicating that about 80% or more of transplanted hADMPCs could differentiated into human albumin-positive hepatocyte-like cells 12 weeks after transplantation. Next, to confirm the differentiation of hADMPCs into hepatocytes *in vivo*, expression of hepatocyte markers was analyzed by quantitative RT-PCR. The WHHL rabbit liver that was transplanted with hADMPCs expressed higher levels of human-specific alpha-1-antitrypsin, albumin, and coagulation factor IX than hADMPCs (Fig. 4C). The expression levels of human GATA-4, human hepatocyte nuclear factor 3 beta, and LDL-receptor were also higher in the WHHL rabbit liver than hADMPCs (Fig. 4C). These results indicate that hADMPCs differentiate into mature hepatocytes *in vivo*.

Discussion

We have used the WHHL rabbit to study the ability of hADMPC-derived hepatocytes to lower serum cholesterol in an animal model of FH. Our results have shown that hADMPCs transplanted into the rabbit liver differentiate into hepatocytes *in vivo* and effectively clear LDL from the circulation.

The reductions in cholesterol brought about by the engrafted hADMPC-derived hepatocytes suggest that human LDL receptors can act as replacement for the mutant LDL receptors in the WHHL rabbit. This capacity of hADMPC-derive hepatocytes is not unexpected, as the liver is the most important site of LDL uptake, accounting for >50% of total removal from the circulation, and the liver is only organ capable of converting cholesterol to bile for excretion. The substantial decrease in serum cholesterol achieved suggests that the hADMPC-derived hepatocytes both internalize LDL and metabolize the cholesterol to bile for excretion. The correlation between cholesterol and coronary heart disease has been well documented, and decreases in serum cholesterol of the magnitude that we have demonstrated would be expected to decrease morbidity and mortality in the patients with severe FH.[25]

The appearance of the hADMPC-derived hepatocytes as revealed by immunohistochemistry and RT-PCR indicated that the hADMPCs differentiated into hepatocytes and integrated into the liver parenchyma. The perivenous migration of the differentiated hepatocytes derived from hADMPCs along the portal-venous axis and suggests that hADMPCs recognize conserved signals on host cells and matrix. There are some reports describing the hepatogenic differentiation potential of hADMPCs.[15,16] These studies

described that hepatocytes differentiated from hADMPCs *ex vivo* engrafted in the liver and functioned, and that the hADMPCs could be resided and changed their characters into hepatocyte-like cells only in the chemically damaged liver. These reports, revealing that hADMPCs have capabilities to differentiate into hepatocytes, hinted us that hADMPCs might differentiate into hepatocytes in liver. Hepatogenic signals from the microenvironment such as cell-to-cell connections or intermediates are probably important factors that dictate the type of functional hepatocytes in hepatic differentiation.[26] We are currently investigating the mechanism for the differentiation hADMPCs into hepatocytes.

The choice of cell source is critical for realizing success in cellular therapy. Liposuction surgeries yield a massive amount of lipoaspirate adipose tissue from 100 mL to >3 L as cell sources.[27] A major advantage of hADMPCs is their availability in safe and easy with few ethical issues, as compared with the shortage of human livers for orthotopic transplantation, which has been shown to be effective for the treatment of FH.[25] Our serum cholesterol reduction studies and *in vitro* studies demonstrated that human LDL binds to the hADMPC-derived hepatocytes receptor, indicating that this therapy will be useful in humans. Previous attempts to study the efficacy of hepatocyte transplantation in the WHHL rabbit model have employed allogenic hepatocytes, xenogenic hepatocytes, or hepatocytes transduced *ex vivo* with a recombinant retrovirus containing the LDL receptor cDNA.[6–13] The lowering effects of hepatocyte transplantation on serum cholesterol have been reported, but there was some problems. First, hepatocytes could not be expanded *ex vivo* with functional potentials; second, the cell viability reduced after cryopreservation; third, the many injected hepatocytes are supposed to be cleared by the reticuloendothelial system or lose viability during early phase. The rate of LDL clearance was returned to normal in LDL receptor knockout mice by introduction of an adenoviral construct containing an LDL receptor cDNA, and similar approaches have lowered serum cholesterol levels in the WHHL rabbit.[10,12,13] However, sustained expression of the LDL receptor from viral vectors can be difficult to achieve.[11,13] Moreover, hepatocytes derived from hADMPCs have the advantage that the LDL receptor is expressed from an endogenous gene with intact regulatory sequences. Such control of LDL receptor levels would not be expected after treatment of hypercholesterolemia with LDL receptor cDNA construct that lack the regulatory regions of the gene.[28]

Our experiments have shown that the hADMPCs expressed hepatocyte markers after transplantation *in vivo* and the integrated cells into parenchyma provide functional LDL receptors, indicating that they differentiated into hepatocytes and might lower serum cholesterol in the WHHL rabbit. These results suggested that hADMPC transplantation via portal vein could correct the metabolic defects of FH patients and that hADMPC-derived hepatocytes could function as supplier with plasma proteins derived from liver, giving us an idea that hADMPC-transplantation might be a novel cell therapy for hemophilia, alpha-1 antitrypsin deficiency, mucolipidosis, and other diseases caused by genetic defects for liver function. In near future, the therapy will be a novel therapy for kinds of inherited liver diseases.

Acknowledgments

This study was supported in part by the Program for Promotion of Fundamental Studies in Health Sciences of the National Institute of Biomedical Innovation (NIBIO), RIKEN Program for Drug Discovery and Medical Technology Platforms, and Kobe Translational Research Cluster, the Knowledge Cluster Initiative, Ministry of Education, Culture, Sports, Science and Technology (MEXT).

Disclosure Statement

All of the authors stated no conflict of interest.

References

1. Brown, M.S., and Goldstein, J.L. A receptor-mediated pathway for cholesterol homeostasis. Science **232,** 34, 1986.
2. Havel, R.J., Yamada, N., and Shames, D.M. Watanabe heritable hyperlipidemic rabbit. Animal model for familial hypercholesterolemia. Arteriosclerosis **9(1 Suppl),** I33, 1989.
3. Yamamoto, T., Bishop, R.W., Brown, M.S., Goldstein, J.L., and Russell, D.W. Deletion in cysteine-rich region of LDL receptor impedes transport to cell surface in WHHL rabbit. Science **32,** 1230, 1986.
4. Bujo, H., Takahashi, K., Saito, Y., Maruyama, T., Yamashita, S., Matsuzawa, Y., Ishibashi, S., Shionoiri, F., Yamada, N., and Kita, T. Clinical features of familial hypercholesterolemia in Japan in a database from 1996–1998 by the research committee of the ministry of health, labour and welfare of Japan. J Atheroscler Thromb **11,** 146, 2004.
5. Yamashita, S., Hbujo, H., Arai, H., Harada-Shiba, M., Matsui, S., Fukushima, M., Saito, Y., Kita, T., and Matsuzawa, Y. Long-term probucol treatment prevents secondary cardiovascular events: a cohort study of patients with heterozygous familial hypercholesterolemia in Japan. J Atheroscler Thromb **15,** 292, 2008.
6. Gunsalus, J.R., Brady, D.A., Coulter, S.M., Gray, B.M., and Edge, A.S. Reduction of serum cholesterol in Watanabe rabbits by xenogeneic hepatocellular transplantation. Nat Med **3,** 48, 1997.
7. Tejera, M.L., Cienfuegos, J.A., Maganto, P., Pardo, F., Santamaria, L., Codesal, J., De Andres, S., Hernandez, J.L., and Castillo-Olivares, J.L. Reduction of cholesterol levels following liver cell grafting in hyperlipidemic (WHHL) rabbits. Transplant Proc **24,** 160, 1992.
8. Wang, J., Pollak, R., and Bartholomew, A. Sustained reduction of serum cholesterol levels following allo-transplantation of parenchymal hepatocytes in Watanabe rabbits. Transplant Proc **23,** 894, 1991.
9. Wiederkehr, J.C., Kondos, G.T., and Pollak, R. Hepatocyte transplantation for the low-density lipoprotein receptor-deficient state. A study in the Watanabe rabbit. Transplantation **50,** 466, 1990.
10. Chowdhury, J.R., Grossman, M., Gupta, S., Chowdhury, N.R., Baker, J.R., Jr., and Wilson, J.M. Long-term improvement of hypercholesterolemia after *ex vivo* gene therapy in LDLR-deficient rabbits. Science **254,** 1802, 1991.
11. Ishibashi, S., Brown, M.S., Goldstein, J.L., Gerard, R.D., Hammer, R.E., and Herz, J. Hypercholesterolemia in low density lipoprotein receptor knockout mice and its reversal by adenovirus-mediated gene delivery. J Clin Invest **92,** 883, 1993.
12. Kozarsky, K.F., McKinley, D.R., Austin, L.L., Raper, S.E., Stratford-Perricaudet, L.D., and Wilson, J.M. *In vivo* correction

of low density lipoprotein receptor deficiency in the Watanabe heritable hyperlipidemic rabbit with recombinant adenoviruses. J Biol Chem **269,** 13695, 1994.
13. Wilson, J.M., Chowdhury, N.R., Grossman, M., Wajsman, R., Epstein, A., Mulligan, R.C., and Chowdhury, J.R. Temporary amelioration of hyperlipidemia in low density lipoprotein receptor-deficient rabbits transplanted with genetically modified hepatocytes. Proc Natl Acad Sci U S A **87,** 8437, 1990.
14. Okura, H., Komoda, H., Saga, A., Kakuta-Yamamoto, A., Hamada, Y., Fumimoto, Y., Lee, C.M., Ichinose, A., Sawa, Y., and Matsuyama, A. Properties of hepatocyte-like cell clusters from human adipose tissue-derived mesenchymal stem cells. Tissue Eng Part C Methods **16,** 761, 2010.
15. Banas, A., Teratani, T., Yamamoto, Y., Tokuhara, M., Takeshita, F., Quinn, G., Okochi, H., and Ochiya, T. Adipose tissue-derived mesenchymal stem cells as a source of human hepatocytes. Hepatology **46,** 219, 2007.
16. Seo, M.J., Suh, S.Y., Bae, Y.C., and Jung, J.S. Differentiation of human adipose stromal cells into hepatic lineage *in vitro* and *in vivo*. Biochem Biophys Res Commun **328,** 258, 2005.
17. Komoda, H., Okura, H., Lee, C.M., Sougawa, N., Iwayama, T., Hashikawa, T., Saga, A., Yamamoto, A., Ichinose, A., Murakami, S., Sawa, Y., and Matsuyama, A. Reduction of N-glycolylneuraminic acid xenoantigen on human adipose tissue-derived stromal cells/mesenchymal stem cells leads to safer and more useful cell sources for various stem cell therapies. Tissue Eng Part A **16,** 1143, 2010.
18. Okura, H., Matsuyama, A., Lee, C.M., Saga, A., Kakuta-Yamamoto, A., Nagao, A., Sougawa, N., Sekiya, N., Takekita, K., Shudo, Y., Miyagawa, S., Komoda, H., Okano, T., and Sawa, Y. Cardiomyoblast-like cells differentiated from human adipose tissue-derived mesenchymal stem cells improve left ventricular dysfunction and survival in a rat myocardial infarction model. Tissue Eng Part C Methods **16,** 417, 2010.
19. Bjorntorp, P., Karlsson, M., Pertoft, H., Pettersson, P., Sjostrom, L., and Smith, U. Isolation and characterization of cells from rat adipose tissue developing into adipocytes. J Lipid Res **19,** 316, 1978.
20. Zuk, P.A., Zhu, M., Ashjian, P., De Ugarte, D.A., Huang, J.I., Mizuno, H., Alfonso, Z.C., Fraser, J.K., Benhaim, P., and Hedrick, M.H. Human adipose tissue is a source of multipotent stem cells. Mol Biol Cell **13,** 4279, 2002.
21. Nicklas, J.A., and Buel, E. Development of an Alu-based, real-time PCR method for quantitation of human DNA in forensic samples. J Forensic Sci **48,** 936, 2003.
22. Opel, K.L., Fleishaker, E.L., Nicklas, J.A., Buel, E., and McCord, B.R. Evaluation and quantification of nuclear DNA from human telogen hairs. J Forensic Sci **53,** 853, 2008.
23. Okazaki, M., Usui, S., Ishigami, M., Sakai, N., Nakamura, T., Matsuzawa, Y., and Yamashita, S. Identification of unique lipoprotein subclasses for visceral obesity by component analysis of cholesterol profile in high-performance liquid chromatography. Arterioscler Thromb Vasc Biol **25,** 578, 2005.
24. Bier, D.M., and Havel, R.J. Activation of lipoprotein lipase by lipoprotein fractions of human serum. J Lipid Res **11,** 565, 1970.
25. Steinberg, D., and Witztum, J.L. Current concepts. Lipoproteins and atherogenesis. Current concepts. JAMA **264,** 3047, 1990.
26. Hughes, R.D., Mitry, R.R., and Dhawan, A. Hepatocyte transplantation for metabolic liver disease: UK experience. J R Soc Med **98,** 341, 2005.
27. Gimble, J.M., Katz, A.J., and Bunnell, B.A. Adipose-derived stem cells for regenerative medicine. Circ Res **100,** 1249, 2007.
28. Bilheimer, D.W., Goldstein, J.L., Grundy, S.M., Starzl, T.E., and Brown, M.S. Liver transplantation to provide low-density-lipoprotein receptors and lower plasma cholesterol in a child with homozygous familial hypercholesterolemia. N Engl J Med **311,** 1658, 1984.

Address correspondence to:
Akifumi Matsuyama, M.D., Ph.D.
Department of Somatic Stem Cell Therapy and Health Policy
Foundation for Biomedical Research and Innovation
TRI305, 1-5-4 Minatojima-minamimachi, Chuo-ku
Kobe 650-0047
Japan

E-mail: akifumi-matsuyama@umin.ac.jp

Received: March 7, 2010
Accepted: August 9, 2010
Online Publication Date: September 21, 2010

Analytical Biochemistry 421 (2012) 595–606

Contents lists available at SciVerse ScienceDirect

Analytical Biochemistry

journal homepage: www.elsevier.com/locate/yabio

One-pot characterization of cancer cells by the analysis of mucin-type glycans and glycosaminoglycans

Keita Yamada [a,b], Yosuke Mitsui [a], Naotaka Kakoi [a], Mitsuhiro Kinoshita [a], Takao Hayakawa [c], Kazuaki Kakehi [a,*]

[a] School of Pharmacy, Kinki University, Higashi-Osaka, Osaka 577-8502, Japan
[b] Division of Glyco-Bioindustry, Life Science Research Center, Institute of Research Promotion, Kagawa University, Miki-cho, Kita-gun, Kagawa 761-0793, Japan
[c] Pharmaceutical Research and Technology Institute, Kinki University, Higashi-Osaka, Osaka 577-8502, Japan

ARTICLE INFO

Article history:
Received 14 September 2011
Received in revised form 5 December 2011
Accepted 8 December 2011
Available online 14 December 2011

Keywords:
Mucin-type glycans
Glycosaminoglycans
Serotonin affinity chromatography
Capillary electrophoresis
MALDI–TOF MS
Cancer cells

ABSTRACT

We developed an automated apparatus for rapid releasing of *O*-glycans from mucin-type glycoproteins [Anal. Biochem. 371 (2007) 52–61; Anal. Chem. 82 (2010) 7436–7443] and applied the device to analyze them in some cancer cell lines [J. Proteome Res. 8 (2009) 521–537]. We also found that the device is useful to release glycosaminoglycans from proteoglycans [Anal. Biochem. 362 (2007) 245–251]. Based on these studies, we developed a method for one-pot analysis of mucin-type glycans and glycosaminoglycans after releasing them from total protein pool obtained from some cancer cell lines. Mucin-type glycans were analyzed by a combination of high-performance liquid chromatography and mass spectrometry techniques, and glycosaminoglycans were analyzed by capillary electrophoresis as fluorescent-labeled unsaturated disaccharides after digestion with specific eliminases followed by fluorescent labeling. Ten cancer cell lines, including blood cancer cells as well as epithelial cancer cells, were used to assess the method. The results clearly revealed that both mucin-type glycans and glycosaminoglycans showed quite interesting profiles. Thus, the current technique will be a powerful tool for discovery of glycan markers of diseases.

© 2011 Elsevier Inc. All rights reserved.

Analysis of glycan structures has become one of the requirements of postgenomic research. Most of the glycans attached to glycoproteins are classified into *N*- and *O*-glycans. Because of the extremely complex structures and heterogeneity of both *N*- and *O*-glycans, we often need to analyze their structures after releasing them from the core protein. In the analysis of *N*-glycans, *N*-glycoamidase having broad specificity is generally used to release *N*-glycans from the peptide backbone. We reported two methods for the analysis of *N*-glycans by labeling with 9-fluorenylmethyl chloroformate and 2-aminobenzoic acid (2AA)[1] [1,2]. These two methods allow sensitive analysis of *N*-glycans by high-performance liquid chromatography (HPLC), capillary electrophoresis (CE), and mass spectrometry (MS). We also achieved comprehensive analysis of *N*-glycans in various cancer cell lines and antibody pharmaceuticals [2,3].

In contrast, structural and quantitative analysis of *O*-glycans attached to the mucin-type glycoproteins has been a difficult task due to lack of appropriate *O*-glycan releasing methods. β-Elimination under mild alkaline conditions is still commonly employed but requires long reaction times. In addition, reducing reagents such as sodium borohydride need to be added to prevent unwanted degradation of the released glycans (i.e., peeling) [4–6]. This causes a loss of the original reducing terminal, and the released glycans do not have an aldehyde group, which is important for sensitive detection and high-resolution analysis by labeling with sensitive fluorescent or chromophoric reagents.

Release of *O*-glycans with the intact reducing end has been reported. Royle and coworkers employed mild hydrazinolysis to afford free *O*-glycans from microgram quantities of glycoproteins, but a lengthy reaction time and reacetylation of de-N-acetylated groups are required [7]. Huang and coworkers developed a method for releasing *O*-glycans in the presence of ammonia, but the method also requires a long reaction time [8].

Recently, we developed an automatic *O*-glycan releasing apparatus to obtain *O*-glycans from core proteins as free form. The apparatus enables release of *O*-glycans within only 3 min without significant degradations of the released glycans. In addition, our method showed excellent repeatability [9,10]. We also connected

* Corresponding author. Fax: +81 6 6721 2353.
E-mail address: k_kakehi@phar.kindai.ac.jp (K. Kakehi).

[1] *Abbreviations used:* 2AA, 2-aminobenzoic acid; HPLC, high-performance liquid chromatography; CE, capillary electrophoresis; MS, mass spectrometry; MALDI–TOF, matrix-assisted laser desorption/ionization time-of-flight; GAG, glycosaminoglycan; HS, heparan sulfate; HA, hyaluronic acid; DHB, 2,5-dihydroxybenzoic acid; $NaBH_4$, sodium borohydride; PBS, phosphate-buffered saline; MWCO, molecular weight cutoff; NP-HPLC, normal phase HPLC; MS/MS, tandem MS; CS, chondroitin sulfate.

0003-2697/$ - see front matter © 2011 Elsevier Inc. All rights reserved.
doi:10.1016/j.ab.2011.12.017

this system to an automatic spotter (AccuSpot from Shimadzu) for direct matrix-assisted laser desorption/ionization time-of-flight (MALDI–TOF) MS measurement for routine analysis of O-glycans, and the analysis of the released O-glycans is completed within 1.5 h [11].

During the releasing reaction, we found that glycosaminoglycans (GAGs) are also conveniently released from proteoglycans. The released GAGs are digested with specific eliminases to produce a mixture of unsaturated disaccharides that are conveniently labeled with a fluorescent tag such as 2AA or 2-aminoacridone and analyzed by CE [12].

These two types of O-glycans (mucin-type glycans and GAGs) are concerned with various biological functions [13–16], and there are a number of research works on the aberrant glycan patterns in relation to progression of diseases [17–20]. Structural alterations of mucin-type glycans are often observed in tumors. For example, core 3 and core 4 mucin-type glycans are synthesized in normal cells but apparently down-regulated in gastric and colorectal carcinoma [21,22] (see Supplementary Fig. 1 in supplementary material for the core structures of O-glycans). Iwai and coworkers showed that expression of the enzymes related to the synthesis of core 3 structure reduced tumor formation in human fibrosarcoma cells [22]. Cancer-associated mucin-type glycans were highly sialylated but less sulfated and were often truncated [23–25]. Truncated mucin-type glycans such as Tn and T antigens as well as their sialylated analogues became predominant with the progression of cancer [26]. The occurrence of the sialyl-Lewis^x (NeuAcα2-3Galβ1-4(Fucα1-3)GlcNAcβ1-3Gal-R:SLe^x) epitope on O-glycans in colon cancer patients is also associated with poor survival [27]. In addition, metastatic cancer cells often express the increased amounts of sialyl-Lewis^a epitope (NeuAcα2-3Galβ1-3(Fucα1-4)GlcNAcβ1-3Gal-R:SLe^a) and SLe^x [28,29].

Many reports on the alterations of GAGs in relation to tumorigenesis have also appeared. Nonsulfated chondroitin is detected in tumor tissues, whereas it is almost absent in normal specimens [30]. Furthermore, differences in the sulfation pattern of heparan sulfate (HS) were also reported [31]. For example, HS from lung cancer cells exhibited a higher degree of oversulfation that was due to an increased content of the three repeating disaccharides having 6-O-sulfated glucosamine residues [31]. Highly sulfated HS acts as a coreceptor for a variety of pro-angiogenic factors, such as vascular endothelial growth factor and fibroblast growth factor, and plays vital roles throughout the various stages of angiogenesis and tumor growth [32–34]. Increased levels of hyaluronic acid (HA) are also associated with certain types of human primary and metastatic cancers [35,36]. Vizoso and coworkers measured the expression level of HA in gastric tumor tissues from 129 patients, and they revealed that high expression of HA is an indicator of poor prognosis for patients with gastric cancer [37].

Glycans are not the direct products by genes; rather, they are the product by a combination of actions of the relevant enzymes. Therefore, alteration of structure simultaneously occurs in some glycans, and comprehensive analysis of glycan structures is required to reveal the relationship between biological characteristics and glycans. Two types of these O-glycans described above were commonly attached to serine (or threonine) residues on peptides and can be affected with each other. Based on these considerations, determination of alterations of multiple kinds of glycans will lead to accurate understanding of diseases, including tumors.

Unfortunately, it should be noticed that profiles of mucin-type O-glycans and GAGs have been reported independently. In addition, there is little information on the relationship between the changes of mucin-type O-glycans and GAGs. If we can obtain both types of information at the same time, the amount of knowledge on both glycans can increase dramatically and will be an important tool for cancer diagnostics and therapies. Based on these considerations, this study aimed at one-pot analysis of mucin-type O-glycans and GAGs.

Materials and methods

Materials

Pronase (*Streptomyces griseus*) was obtained from Calbiochem (San Diego, CA, USA). 2AA and sodium cyanoborohydride for fluorescent labeling of the released glycans were obtained from Tokyo Kasei (Tokyo, Japan) and Sigma–Aldrich Japan (Tokyo, Japan), respectively. Sephadex LH-20 was obtained from GE Healthcare (Tokyo, Japan). Triton X-100, 2,5-dihydroxybenzoic acid (DHB), and sodium borohydride ($NaBH_4$) were also obtained from Sigma–Aldrich Japan. Protein inhibitor cocktail for animal cells was obtained from Nacalai Tesque (Kyoto, Japan). A serotonin-immobilized column for the separation of sialo glycans was obtained from Seikagaku Biobusiness (Tokyo, Japan). Chondroitinase ABC, heparitinase 1, heparitinase 2, and standard samples of unsaturated disaccharides for the analysis of GAGs were also obtained from Seikagaku Biobusiness. Fused silica capillary tubing (50 μm i.d.) was obtained from GE Healthcare. Other reagents and solvents were of the highest grade commercially available or HPLC grade. All aqueous solutions were prepared using water purified with a Milli-Q purification system (Millipore, Bedford, MA, USA).

Cell cultures

In the current study, human-derived cancer cells were employed: U937 (histiocytic lymphoma), K562 (chronic myelogenous leukemia), Jurkat (acute T cell leukemia), HL-60 (acute promyelocytic leukemia), LS174T (colorectal adenocarcinoma), HCT116 (colorectal adenocarcinoma), HCT15 (colorectal adenocarcinoma), BxPC3 (pancreatic adenocarcinoma), PANC1 (pancreatic carcinoma), and MKN7 and MKN45 (gastric adenocarcinoma). All of these cells except LS174T were cultured in RPMI 1640 medium supplemented with 10% (v/v) fetal calf serum and 1% (v/v) penicillin/streptomycin mixed solution (10,000 U/ml penicillin and 10 mg/ml streptomycin, Nacalai Tesque). LS174T cells were cultured in minimum essential medium supplemented with 10% (v/v) fetal calf serum. Fetal calf serum was previously kept at 56 °C for 30 min. The cells were cultured at 37 °C under 5% CO_2 atmosphere and harvested at 80% confluent state. Collected cells (1.0×10^7 cells) were washed with phosphate-buffered saline (PBS) and collected by centrifugation at 1000 rpm for 20 min.

Glycopeptide pool from whole cells

Glycopeptide pool derived from cancer cells was prepared according to the method reported previously [38]. Cultured cells (1.0×10^7 cells) were suspended in 5 mM Tris–HCl buffer (pH 8.0, 500 μl) and mixed with an equal volume of 2% Triton X-100 in the same buffer in an ice bath. After homogenizing the cells for 7 min with a glass homogenizer, the mixture was centrifuged at 8000*g* for 30 min. The supernatant layer was collected and boiled for 7 min at 100 °C and evaporated to dryness by a centrifugal evaporator (SpeedVac, Savant, Sunnydale, CA, USA). The lyophilized material was suspended in water (200 μl), and ethanol (800 μl) was added to the mixture to 80% concentration. The precipitate was collected by centrifugation and washed with ethanol (1 ml × 3) and then with acetone (1 ml × 2), followed by drying in vacuo. The residue was digested with pronase (50 μg) in 50 mM Tris–HCl (pH 8.0, 200 μl) at 37 °C for 24 h. The reaction mixture was boiled for 10 min, and the supernatant was collected after centrifugation. Because free glycans present in some cancer cells inhibit the subsequent analysis of O-glycans [39], reduction

with $NaBH_4$ prior to *O*-glycan releasing reaction is necessary. An aqueous solution of 2 M $NaBH_4$ (500 μl) was added to the supernatant and kept at room temperature for 30 min. Glacial acetic acid was carefully added to the mixture to decompose excess $NaBH_4$, and the mixture was passed through an ultrafiltration membrane (5000 MWCO [molecular weight cutoff], Amicon Ultra, Millipore) at 10,000*g*. The mixture of glycopeptides on the membrane was dissolved in water (100 μl) and used for releasing reaction of *O*-glycans from mucin-type glycoproteins and proteoglycans.

Releasing reactions of O-glycans

Releasing reaction of *O*-glycans using the automated glycan releasing system was performed according to the method reported previously [9]. Briefly, an aqueous solution of 0.5 M LiOH was used as the releasing reagent and the eluent. To the flow of the eluent at 1.0 ml/min, an aqueous solution of the mixture of glycopeptides from each cell line (5.0×10^6 cells/50 μl) obtained as described above was injected. After the sample solution was mixed with the eluent in the mixing device, the mixed solution was moved to the reactor kept at 60 °C, in which a reaction tube (0.25 mm i.d., 10 m length, 700 μl volume) was set. During passing through the reaction tube in the reactor, *O*-glycans were released from the peptide. The eluate containing the reaction mixture from the reactor was immediately introduced to a cartridge (1.0 ml volume) packed with cation exchange resin and collected to a fraction collector installed in the system while monitoring the absorbance at 230 nm. The collected solution containing the released *O*-glycans was evaporated to dryness by a centrifugal evaporator, and the dried material was used for fluorescent labeling with 2AA.

Fluorescent labeling of the released O-glycans with 2AA

The mixture of the released *O*-glycans was dissolved in 2AA solution (200 μl), which was freshly prepared by dissolution of 2AA (30 mg) and sodium cyanoborohydride (30 mg) in methanol (1 ml) containing 4% sodium acetate and 2% boric acid. The mixture was kept at 80 °C for 1 h. After cooling, water (100 μl) was added and the mixture was applied to a column of Sephadex LH-20 (1.0 cm i.d., 30 cm length) previously equilibrated with 50% aqueous methanol. The earlier eluted fluorescent fractions were pooled and evaporated to dryness under reduced pressure. The dried residue was dissolved in water (40 μl), and a portion (20 μl) was injected to analyze by serotonin affinity chromatography.

Serotonin affinity chromatography for separation of O-glycans and GAGs

Mucin-type glycans and GAGs are analyzed according to the procedures (see Supplementary Fig. 2 in supplementary material). Serotonin affinity chromatography for group separation of glycans based on the number of attached sialic acid residues was performed with a Jasco HPLC apparatus equipped with two PU-980 pumps and a Jasco FP-920 fluorescence detector (Tokyo, Japan) using a serotonin-immobilized column (4.6 × 150 mm) with linear gradient from water (solvent A) to 50 mM ammonium acetate (solvent B) at a flow rate of 0.5 ml/min. Initially solvent B was used at 5% concentration for 2 min, and then linear gradient elution was performed to 37% B for 16 min. After collecting mucin-type glycans, an aqueous solution of 1 M NaCl was used to elute GAGs during the subsequent 15 min. The column was then equilibrated with the starting eluent. After group separation, mucin-type glycan fractions were analyzed by MALDI–TOF MS and normal phase HPLC (NP–HPLC). In addition, GAG fractions were digested with specific eliminases and analyzed by CE after labeling with 2AA.

HPLC analysis of mucin-type glycans

The apparatus was the same as described above. Separation was done with a TSK-GEL Amide-80 column (Tosoh, 4.6 × 250 mm) using a linear gradient formed by 0.1% acetic acid in acetonitrile (solvent A) and 0.2% acetic acid in water containing 0.1% triethylamine (solvent B) at 40 °C. The column was initially equilibrated and eluted with 85% solvent A for 2 min, from which point solvent B was increased to 50% over 80 min at 1.0 ml/min. Then, the column was washed with 90% B for 10 min and equilibrated at initial conditions for 15 min. The amounts of mucin-type glycans were calculated from the peak areas based on the standard curve prepared using maltopentaose labeled with 2AA.

MALDI–TOF MS analysis of mucin-type glycans separated by serotonin affinity chromatography

MALDI–TOF MS spectra of 2AA-labeled glycans were acquired on a Voyager-DE Pro mass spectrometer (PE Biosystems, Framingham, MA, USA) in negative or positive ion linear mode with a nitrogen laser (338 nm) for the ionization source. Accelerating voltage was set at 20 kV, and delayed extraction was performed after 800 ns. DHB was used as matrix material throughout the work. The mass numbers of the molecular ion peaks were corrected using a mixture of 2AA-labeled dextran oligomers as standard mass markers. The sample solution (1 μl) was mixed with 2% DHB (1 μl) in ethanol on a stainless-steel plate, and the mixture was dried under atmosphere at room temperature.

MS^n analysis of mucin-type glycans

Structures of mucin-type glycans were confirmed by the MS^n technique on a MALDI–quadrupole ion trap–TOF mass spectrometer (AXIMA-Resonance, Shimadzu, Kyoto, Japan). Acquisition and data processing were controlled by Launchpad software (Kratos Analytical, Manchester, UK). For collision-induced dissociation, argon was used as the collision gas. For the sample preparation, a 0.5-μl volume of the matrix solution (DHB, 10 mg/ml in 30% ethanol) was deposited on the stainless-steel target plate and allowed to dry. Then, a portion (0.5 μl) of the appropriately diluted analyte solution (typically ~1 pmol/μl) was applied to cover the matrix on the target plate and allowed to dry.

Analysis of GAGs collected by serotonin affinity chromatography

After collecting the GAG pool by serotonin affinity chromatography, the GAG pool was passed through a filter device (3000 MWCO). Half of the GAG mixture on the membrane was dissolved in 50 mM Tris–HCl buffer (pH 8.0, 100 μl). Chondroitinase ABC (0.5 U) dissolved in the same buffer (10 μl) was added to the solution and kept at 37 °C overnight. The other half of the GAG mixture was dissolved in 100 mM sodium acetate/0.1 mM calcium acetate (pH 7.0, 100 μl). Heparitinases 1 and 2 (5 mU/10 μl each) were added to the solution, and the mixture was kept at 37 °C overnight. Both reaction mixtures obtained by digestion with chondroitinase ABC and heparitinases were labeled with 2AA and analyzed by CE.

CE analysis of unsaturated disaccharides from GAGs

CE was performed on a P/ACE MDQ Glycoprotein System (Beckman Coulter, Fullerton, CA, USA) equipped with a helium–cadmium laser-induced fluorescence detector (excitation 325 nm, emission 405 nm). For the analysis of 2AA-labeled unsaturated disaccharides derived from GAGs, electrophoresis was performed with a fused silica capillary (50 μm i.d. × 30 cm) in 100 mM Tris–phosphate buffer (pH 3.0). Sample solutions were introduced into

the capillary by pressure injection at 1 psi for 10 s. Separation was performed by applying the potential of 25 kV at 25 °C.

The amounts of unsaturated disaccharides were calculated from the peak areas based on the standard curve prepared using standard samples of unsaturated disaccharides labeled with 2AA.

Results and discussion

Separation of mucin-type glycans and GAGs by serotonin affinity chromatography

We have been employing serotonin affinity chromatography for group separation of 2AA-labeled *N*- and mucin-type glycans prepared from various cancer cell lines using gradient elution with ammonium acetate. The separation is achieved based on the number of sialic acid residues [2,38], and the glycans separated in this way are analyzed by HPLC and MS without further purification steps because the glycan fractions are in an aqueous solution of volatile salts at low concentrations. This is one of the advantages of serotonin affinity chromatography.

During the studies on the analysis of the released glycans, we found that GAGs are also retarded on a serotonin-immobilized column (Fig. 1). An example for the analysis of oligomers derived from hyaluronan (HA oligomers) is shown in Fig. 1A. HA oligomers were strongly retained on the serotonin-immobilized stationary phase based on their total negative charges (i.e., oligomers having the higher molecular weight are eluted later). It is considered that glucuronic acid residues in HA molecules play important roles in interaction with serotonin. We also analyzed the artificial mixture of mucin-type glycans from fetuin and HA oligomers (Fig. 1B). Mucin-type glycans from fetuin were observed at 8 and 15 min, and then HA oligomers were observed. The results indicated that serotonin affinity chromatography is useful for group separation of mucin-type glycans and GAGs. Based on these results, we developed the procedures for one-pot analysis of mucin-type glycans and GAGs as described in Materials and methods and applied the method to the analysis of *O*-glycans on HCT116 cells (colorectal adenocarcinoma).

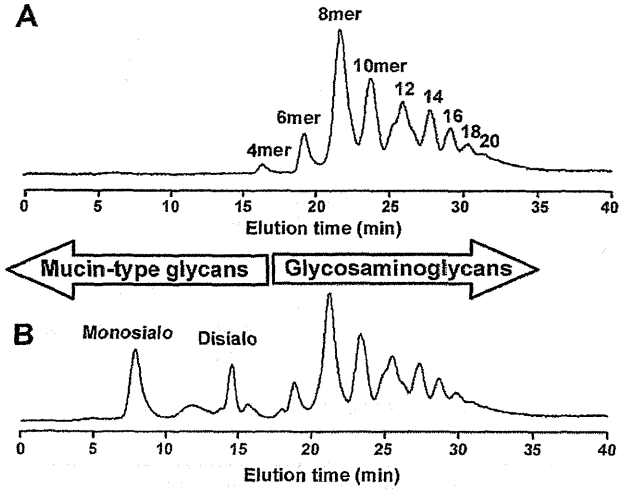

Fig.1. Separation of mucin-type glycans and GAGs by serotonin affinity chromatography. 2AA-labeled HA oligosaccharides (A) and a mixture of HA oligosaccharides and mucin-type glycans derived from bovine fetuin (B) are shown. Analytical conditions: eluent, water (solvent A) and 40 mM ammonium acetate (solvent B); gradient condition, linear gradient (5–75% solvent B) from 2 to 37 min and 75 to 100% solvent B from 37 to 45 min.

One-pot analysis of mucin-type glycans and GAGs from HCT116 cells

In the initial step of the analysis of *O*-glycans expressed on HCT116 cells, the released glycans were separated by serotonin affinity chromatography (Fig. 2). Asialo (M1), monosialo (M2 and M3) and disialo (M4–M6) mucin-type glycans were observed at 3–5, 5.2–10.0, and 10.8–16.0 min, respectively. After all mucin-type glycans were eluted, GAGs were eluted with 1 M NaCl. Each fraction obtained in this way was analyzed according to the method described in Materials and methods.

Six mucin-type glycan fractions (M1–M6) were analyzed by NP–HPLC and MALDI–TOF MS (Fig. 3), and the list of the observed mucin-type glycans in HCT116 cells is summarized in Table 1. The MS data were analyzed by Glycopeakfinder and Glycoworkbench in EUROCarbDB (http://www.ebi.ac.uk/eurocarb/tools.action). The amounts of expressed mucin-type glycans were calculated from the peak areas observed by NP–HPLC. We found 31 mucin-type glycans in HCT116 cells. Asialo glycans, T antigen (*m/z* 503: Galβ1-3GalNAc-2AA), core 2 structure (*m/z* 706: Galβ1-3(GlcNAcβ1-6)GalNAc-2AA), galactosyl core 2 structure (*m/z* 868: Galβ1-3(Galβ1-4GlcNAcβ1-6)GalNAc-2AA), and a polylactosamine-type glycan (*m/z* 1233: $Hex_3HexNAc_3$-2AA) were observed. Tandem MS (MS/MS) analysis of the peak observed at 1233 gave the ions at *m/z* 544 and 503 (Fig. 4A). These ions are obviously due to GlcNAcβ1-6GalNAc-2AA and Galβ1-3GalNAc-2AA (Fig. 4A). Based on these results, the glycan observed at *m/z* 1233 was confirmed as polylactosaminyl core 2 structure, Gal-GlcNAc-Galβ1-4 GlcNAcβ1-6(Galβ1-3)GalNAc-2AA. Monosialo core 1 and core 2 structures were found in monosialo glycan fractions (M2 and M3). Monosialo-polylactosamine-type glycans were also clearly observed in M2. These glycans have polylactosaminyl core 2 structure. Monosialo glycans having smaller molecular sizes such as sialyl-T and monosialo core 2 structure were observed in M3. Disialo core 1, core 2, and disialo-polylactosaminyl glycans were observed in M4, M5, and M6. It should be noted that mono sulfated mucin-type glycans were observed in HCT116 cells. The molecular ion at *m/z* 1604 observed in M6 is due to $NeuAc_1Hex_3HexNAc_3$-2AA + SO_3. After neuraminidase digestion, MS/MS analysis of this glycan afforded a desulfated molecular ion peak at *m/z* 1233 (Fig. 4B, upper spectrum). By MS^3 analysis, the fragment ion peak observed at *m/z* 1233 is confirmed as polylactosaminyl core 2 structure, Gal-GlcNAc-Galβ1-4 GlcNAcβ1-6(Galβ1-3)GalNAc-2AA (Fig. 4B, lower spectrum). In addition, two fragment ion peaks at *m/z* 444 and 948 were observed in MS^2 spectrum (Fig. 4B, upper spectrum). The fragment ion peak at *m/z* 444 corresponds to sulfated lactosamine, GalGlcNAc + SO_3. The fragment ion peak at *m/z*

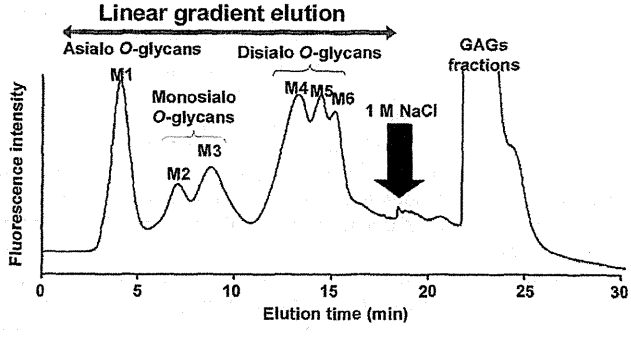

Fig.2. Separation of mucin-type glycans and GAGs derived from HCT116 cells by serotonin affinity chromatography. Analytical conditions: eluent, water (solvent A) and 40 mM ammonium acetate (solvent B); gradient condition, linear gradient (5–41% solvent B) from 2 to 20 min. After collecting the mucin-type glycans, GAGs were eluted with 1 M NaCl.

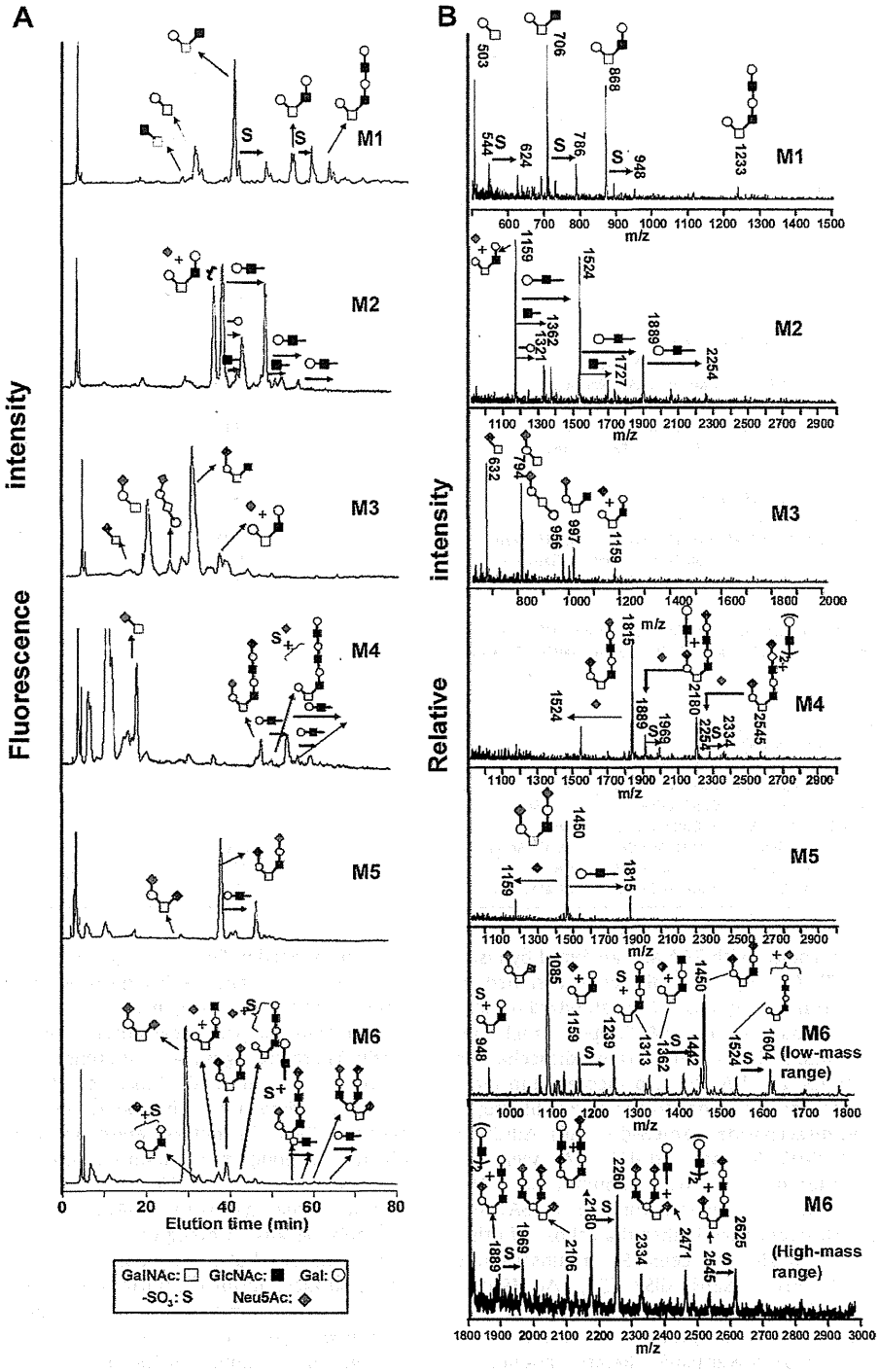

Fig.3. NP–HPLC and MALDI–TOF MS analysis of mucin-type glycans derived from HCT116 cells. The mucin-type glycan fractions separated by serotonin affinity chromatography were analyzed by NP–HPLC (A) and MALDI–TOF MS (B). Analytical conditions of HPLC: column, Amide-80 (Tosoh, 4.6 × 250 nm); solvent A, 0.1% CH_3COOH in acetonitrile; solvent B, 0.2% CH_3COOH–0.1% triethylamine in water; gradient condition, linear gradient (15–65% solvent B) from 2 to 82 min.

948 is due to sulfated galactosyl core 2 structure, Galβ1-4GlcNAcβ1-6(Galβ1-3)GalNAc-2AA + SO_3. This fragment ion indicates that terminal lactosamine is not sulfated. It was reported that GlcNAc-6-*O*-sulfotransferase was expressed and Gal-3-*O*-sulfotransferase was down-regulated in colon cancer cells [40]. Based on these considerations, we concluded that the structure of this sulfate-containing mucin-type glycan was Gal-GlcNAc-Galβ1-4(SO_3-6)GlcNAcβ1-6(Galβ1-3)GalNAc-2AA. These types of sulfated glycans were also observed in M1 and M4.

GAG fractions collected by serotonin affinity chromatography were analyzed as unsaturated disaccharides after digestion with specific eliminases. Half of the fractions were digested with chondroitinase ABC, and the other half were treated with a combination of heparitinases 1 and 2. The mixture of unsaturated disaccharides

Table 1
Mucin-type glycans found in HCT116 cells.

Structure	Observed molecular ion peaks (*m/z*)	Amount of glycans (pmol/L × 10^6 cells)
Asialo glycans		
Galβ1-3GalNAc-2AA	503	67.1
GlcNAcβ1-3GalNAc-2AA	544	0.5
Galβ1-3(GlcNAcβ1-6)GalNAc-2AA	706	142.1
Galβ1-3(Galβ1-4GlcNAcβ1-6)GalNAc-2AA	868	73.9
Galβ1-3(Gal-GlcNAc-Galβ1-4GlcNAcβ1-6)GalNAc-2AA	1233	41.8
Monosialo glycans		
NeuAcα2-6GalNAc-2AA	632	122.8
NeuAcα2-3Galβ1-3GalNAc-2AA	794	180.0
NeuAcα2-3Galβ1-3(GlcNAcβ1-6)GalNAc-2AA	997	294.3
Galβ1-3(Galβ1-4GlcNAcβ1-6)GalNAc-2AA + $NeuAc_1$	1159	191.7
Galβ1-3(GlcNAc-Galβ1-4GlcNAcβ1-6)GalNAc-2AA + $NeuAc_1$	1362	32.5
Galβ1-3(Gal-GlcNAc-Galβ1-4GlcNAcβ1-6)GalNAc-2AA + $NeuAc_1$	1524	120.7
Galβ1-3(GlcNAc-Gal-GlcNAc-Galβ1-4GlcNAcβ1-6)GalNAc-2AA + $NeuAc_1$	1727	34.3
Galβ1-3((Gal-GlcNAc)$_2$-Galβ1-4GlcNAcβ1-6)GalNAc-2AA + $NeuAc_1$	1889	32.8
Galβ1-3((Gal-GlcNAc)$_3$-Galβ1-4GlcNAcβ1-6)GalNAc-2AA + $NeuAc_1$	2254	21.5
Disialo glycans		
NeuAcα2-3Galβ1-3(NeuAcα2-6)GalNAc-2AA	1085	217.3
NeuAc-Galβ1-3(NeuAc-Galβ1-4GlcNAcβ1-6)GalNAc-2AA	1450	199.6
NeuAcα2-3Galβ1-3(NeuAc-Gal-GlcNAc-Galβ1-4GlcNAcβ1-6)GalNAc-2AA	1815	170.1
NeuAcα2-3Galβ1-3(NeuAc-(Gal-GlcNAc)$_2$-Galβ1-4GlcNAcβ1-6)GalNAc-2AA	2180	56.0
NeuAcα2-3Galβ1-3(NeuAc-(Gal-GlcNAc)$_3$-Galβ1-4GlcNAcβ1-6)GalNAc-2AA	2545	18.0
Trisialo glycans		
NeuAc-Gal-GlcNAc-(NeuAc-Gal-GlcNAc)Galβ1-3(NeuAcα2-6)GalNAc-2AA	2106	0.5
NeuAc-Gal-GlcNAc(NeuAc-Gal-GlcNAc)Galβ1-3(NeuAcα2-6)GalNAc-2AA + Gal-GlcNAc	2471	0.2
Sulfate glycans		
HexNAc-HexNAc-2AA + SO_3	624	2.3
Galβ1-3(GlcNAcβ1-6)GalNAc-2AA + SO_3	786	66.6
Galβ1-3(Galβ1-4GlcNAcβ1-6)GalNAc-2AA + SO_3	948	81.0
Galβ1-3(Galβ1-4GlcNAcβ1-6)GalNAc-2AA + NeuAc + SO_3	1239	8.8
Galβ1-3(GlcNAc-Galβ1-4GlcNAcβ1-6)GalNAc-2AA + NeuAc + SO_3	1442	17.7
Galβ1-3(Gal-GlcNAc-Galβ1-4GlcNAcβ1-6)GalNAc-2AA + $NeuAc_1$ + SO_3	1604	19.5
Galβ1-3((Gal-GlcNAc)$_2$-Galβ1-4GlcNAcβ1-6)GalNAc-2AA + $NeuAc_1$ + SO_3	1969	1.4
NeuAcα2-3Galβ1-3(NeuAc-(Gal-GlcNAc)$_2$-Galβ1-4GlcNAcβ1-6)GalNAc-2AA + SO_3	2260	3.2
Galβ1-3((Gal-GlcNAc)$_3$-Galβ1-4GlcNAcβ1-6)GalNAc-2AA + $NeuAc_1$ + SO_3	2334	0.2
NeuAcα2-3Galβ1-3(NeuAc-(Gal-GlcNAc)$_3$-Galβ1-4GlcNAcβ1-6)GalNAc-2AA + SO_3	2625	0.5

obtained in this way was labeled with 2AA and analyzed by laser-induced fluorescence (LIF)–CE (Fig. 5). Peaks were assigned by comparing the migration times with those of the standard unsaturated disaccharides. As shown in Fig. 5A (upper panel), we achieved excellent separation of nine unsaturated disaccharides from chondroitin sulfate (CS) and HA. We also succeeded in separation of seven unsaturated disaccharides from HS (Fig. 5B, upper panel). Five unsaturated disaccharides, ΔdiCS-diS_E (SE), ΔdiCS-6S (6S), ΔdiCS-4S (4S), ΔdiCS-0S (0S), and Δdi-HA (HA), were observed in the mixture after digestion with chondroitinase ABC (Fig. 5A, lower panel; see the list of the structures in Fig. 5A). Relative abundance of Δdi-HA was much higher than those of other unsaturated disaccharides in HCT116 cells. Seven unsaturated disaccharides, ΔdiHS-triS (TriS), ΔdiHS-diS3 (S3), ΔdiHS-diS2 (S2), ΔdiHS-diS1 (S1), ΔdiHS-6S (6S), ΔdiHS-NS (NS), and ΔdiHS-0S (0S), were observed in the mixture digested with a combination of heparitinases 1 and 2 (Fig. 5B, lower panel). Relative abundance of unsulfated HS disaccharide (HS0S) was much higher than those of other unsaturated disaccharides in HCT116 cells. It should be noted that there are no other contaminating peaks due to mucin-type *O*-glycans. From these results, it was revealed that mucin-type glycans as well as GAGs were able to be analyzed in the same sample.

Characterization of cancer cell lines

Based on the results obtained by the analysis of both mucin-type glycans and GAGs in HCT116 cells, we applied the methods to the analysis of both glycans on various cancer cells. The results are summarized in Figs. 6–8. Fig. 6 shows the total amount of mucin-type glycans and GAGs expressed on 10 cancer cell lines. The amounts of the expressed mucin-type glycans and GAGs were calculated from the peak areas observed by NP–HPLC and CE, respectively. There are significant differences in the expression levels of mucin-type glycans and GAGs among leukemia cells and epithelial cells. All leukemia cell lines poorly express both mucin-type glycans and GAGs. In contrast, epithelial cells express large amounts of them, although the amounts of the glycans are conspicuously varied among cell lines. There are 10–100 times larger amounts of mucin-type glycans than GAGs present on cancer cells. This is probably because proteoglycans are not present as conjugates in cell membrane but rather loosely interact with the components of cell surface. During the purification step of whole proteins, some portions of proteoglycans are not collected or the expression level of proteoglycans may be intrinsically lower than that of mucin-type glycans, although further studies are required. In any case, the data indicate that glycans are not dense on the floating blood cells. In contrast, glycans in epithelial cells, which form tumor tissues, are present in high density and seem to show important roles in exchanging intercellular information.

Figs. 7 and 8 show comparisons of relative abundances of mucin-type glycans and unsaturated disaccharides derived from glycosaminoglycans in cancer cells. Fig. 7 shows the glycan profiles obtained from four leukemia cells. All cell lines commonly contained sialyl-T and disialyl-T antigens as major mucin-type glycans. K562 and U937 cells especially contained these two glycans as the major glycans. Although it was difficult to discriminate these two cells only by mucin-type glycan analysis, profiling of GAGs

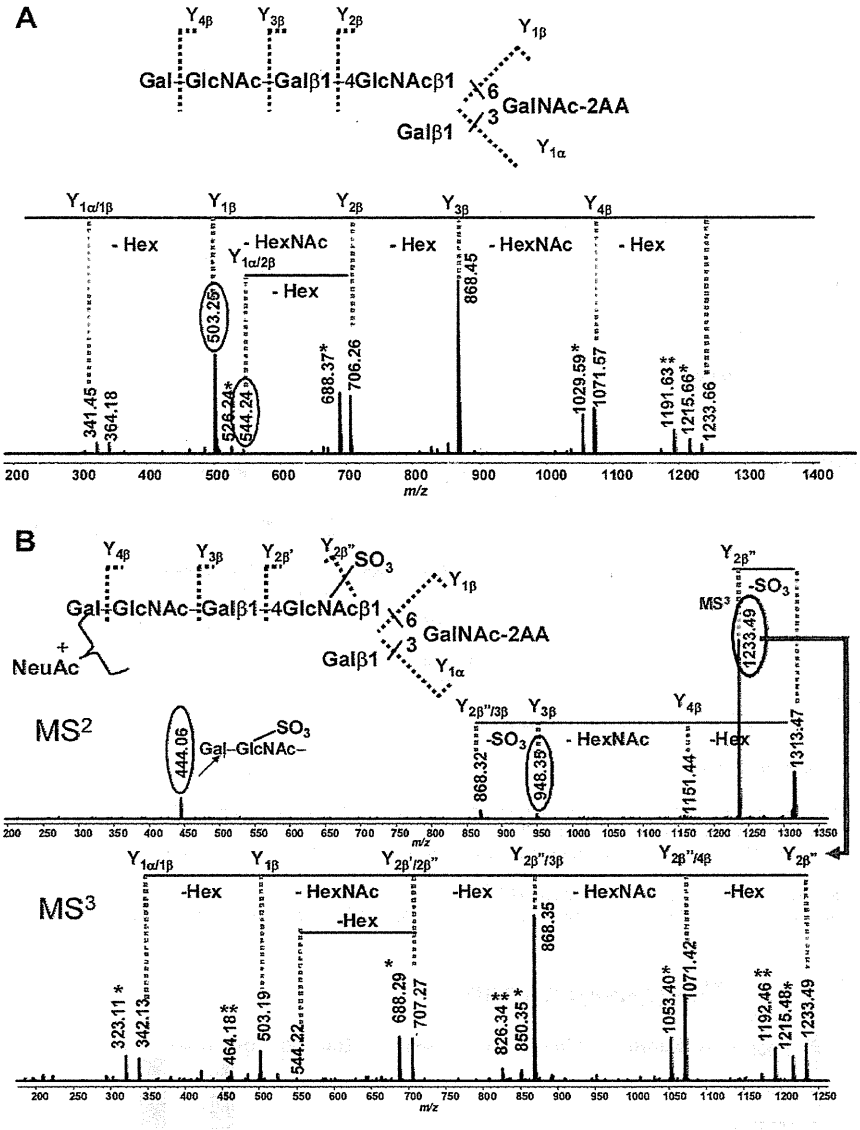

Fig.4. MS/MS analysis of mucin-type glycans derived from HCT116 cells. (A) Polylactosaminyl mucin-type glycan observed at *m/z* 1233. (B) Sulfated mucin-type glycan observed at *m/z* 1604.

could easily discriminate these cells. K562 cells contained ΔdiCS-4S as the major component. In contrast, ΔdiHS-0S was the major component in U937 cells. U937 cells also contained ΔdiCS-4S, but the relative abundance of this unsaturated disaccharide was low. Jurkat cells expressed extremely large amount of Tn antigen. GAGs in Jurkat cells showed profiles similar to those observed in U937 cells. HL-60 cells expressed core 2 mucin-type glycans abundantly. In addition, polylactosaminyl and fucosylated mucin-type glycans were also observed in HL-60 cells. A feature of HL-60 cells is that the cells express elongated mucin-type glycans in comparison with other leukemia cells. ΔdiCS-0S was the major component in HL-60 cells. This means that low-sulfated GAGs were abundant in HL-60 cells.

Fig. 8 shows the results on the characterization of six epithelial cancer cell lines. Mucin-type glycan profiles in epithelial cancer cell lines except PANC1 cells are generally more complex than those of leukemia cancer cells. This means that characterization of mucin-type glycans on epithelial cancer cells will be a powerful tool for correlating with their biological characteristics such as tumorigenesis ability. Sialyl-T and disialyl-T antigens were commonly observed in all cancer cells, although their relative abundances were diverse among cells. However, all cancer cells scarcely expressed core 3 and core 4 structures. These data are well correlated with the reports on down-regulation of these glycans in various tumor tissues [21,22]. Profiles of GAGs also gave interesting results. Relative abundances of HA in epithelial cancer cells were commonly higher than those in leukemia cells. In addition, relative abundances of ΔdiHS-0S also showed higher values than those observed for leukemia cells. These data indicate that sulfation level of HS is significantly low in cancer cell lines. Recently, some research groups reported that HS sulfatases (SULF) are overexpressed in subsets of multiple tumors [41–43]. SULF2 overexpressed in tumor tissues was associated with tumor prognosis [42,44]. These reports indicate that sulfation level of HS is decreased in certain cancer cell lines. Our results are well correlated with these observations. PANC1 cells (poorly differentiated pancreatic cancer cells) expressed sialyl-T and disialyl-T as the major mucin-type glycans. The elongated mucin-type glycans were not

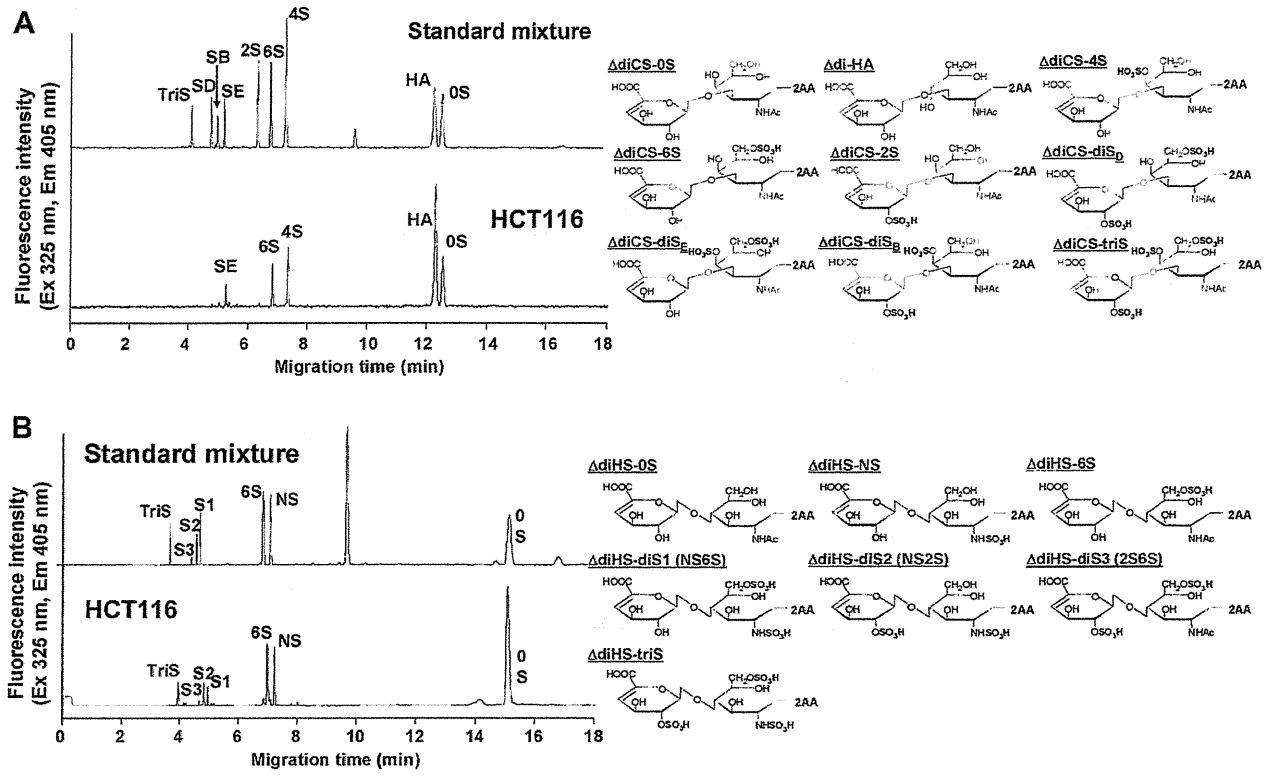

Fig.5. Analysis of unsaturated disaccharides from GAG fractions. 2AA-labeled unsaturated disaccharides of HA and CS (A) and of HS (B) in HCT116 cells were analyzed by CE. Analytical conditions: capillary, fused silica (40 cm × 50 μm i.d); running buffer, 100 mM Tris–phosphate (pH 3.0); applied voltage, 25 kV; injection, pressure method (1.0 psi for 10 s); temperature, 25 °C; detection, He-Cd laser-induced fluorescent detection (excitation 325 nm, emission 405 nm). Abbreviations of unsaturated disaccharide: (A) Unsaturated chondroitin and hyaluronic acid disaccharide: 0S, ΔdiCS-0S (12.8 min); HA, ΔdiHA (12.3 min); 4S, ΔdiCS-4S (7.4 min); 6S, ΔdiCS-6S (6.8 min); 2S, ΔdiCS-2S (6.5 min); SD, ΔdiCS-diS$_D$ (4.8 min); SE, ΔdiCS-diS$_E$ (5.2 min); SB, ΔdiCS-diS$_B$ (5.0 min); TriS, ΔdiCS-triS (4.1 min). (B) Unsaturated heparan sulfate disaccharide: 0S, ΔdiHS-0S (15.3 min); NS, ΔdiHS-NS (7.2 min); 6S, ΔdiHS-6S (6.8 min); S1, ΔdiHS-diS1 (5.0 min); S2, ΔdiHS-diS2 (4.9 min); S3, ΔdiHS-diS3 (4.8 min); TriS, ΔdiHS-TriS (4.0 min).

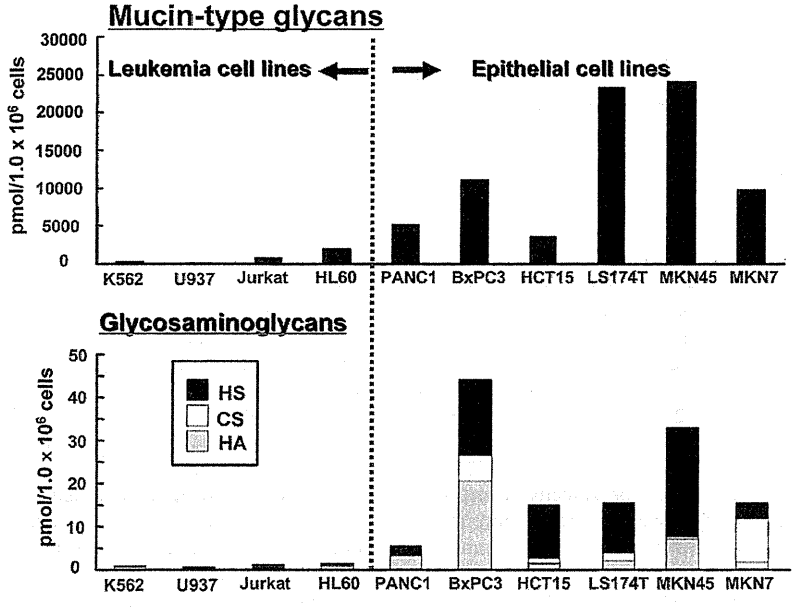

Fig.6. Comparison of the amounts of mucin-type glycans and GAGs expressed on cancer cells. The amounts of the expressed mucin-type glycans and GAGs were calculated from the peak areas observed by NP–HPLC and CE, respectively.

observed in PANC1 cells. Because PANC1 cells lack core 2 β-1,6-*N*-acetylglucosaminyltransferase, which is required for elongation of the mucin-type glycans [45], these observations suggest that tumor-associated epitopes on mucin core proteins expressed on

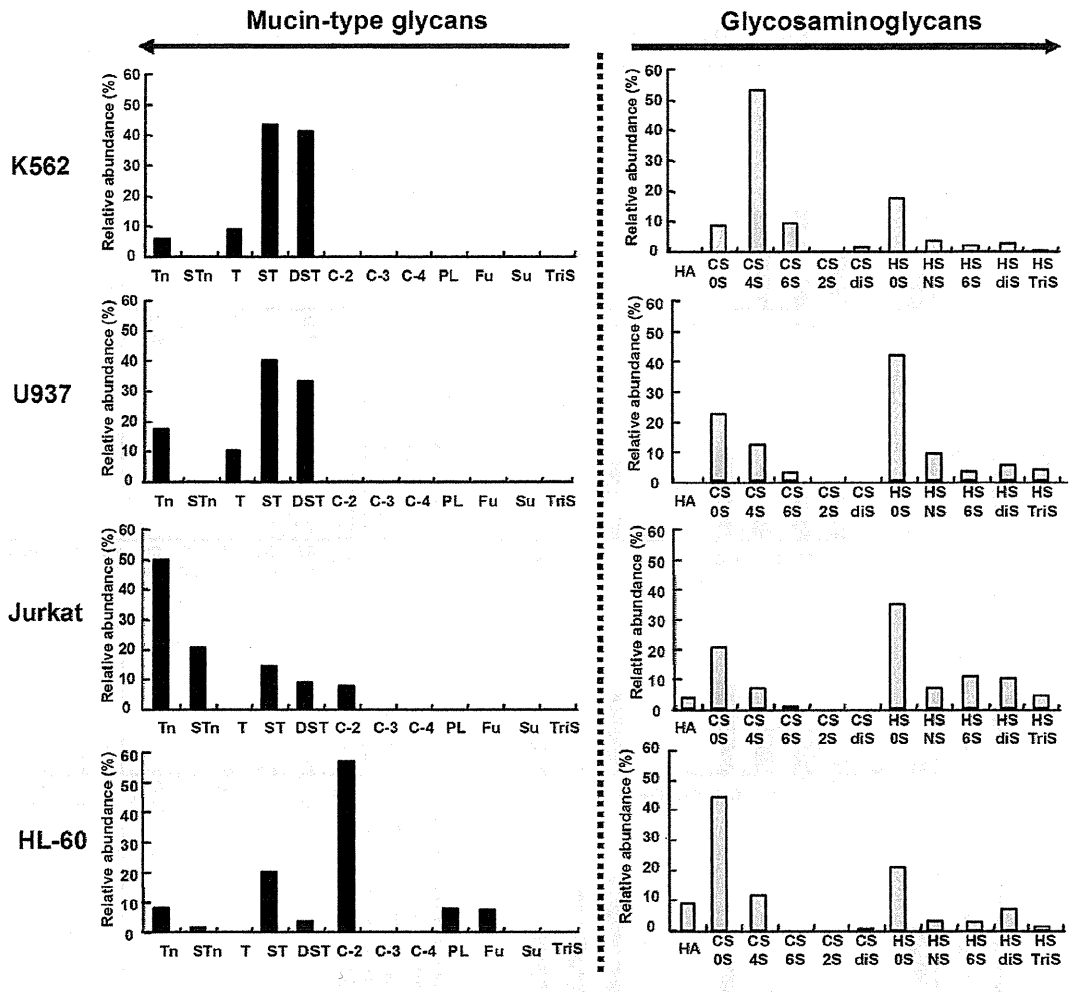

Fig.7. Characterization of four leukemia cell lines. The contents of mucin-type glycans and GAGs are displayed as black bars and gray bars, respectively. Relative abundances of mucin-type glycans and unsaturated disaccharides were calculated from the peak areas observed by NP–HPLC and CE, respectively. Abbreviations: Tn, Tn antigen; STn, sialyl-Tn antigen; T, T antigen; ST, sialyl-T antigen; DST, disialyl-T antigen; C-2, core 2 structure; C-3, core 3 structure; C-4, core 4 structure; PL, polylactosamine-type structure; Fu, fucosylated structure; Su, sulfated structure; TriS, trisialylated structure; HA, Δdi-HA; CS-0S, ΔdiCS-0S; CS-4S, ΔdiCS-4S; CS-6S, ΔdiCS-6S; CS-2S, ΔdiCS-2S; CS-diS, disulfated unsaturated disaccharides of CS; HS-0S, ΔdiHS-0S; HS-NS, ΔdiHS-NS; HS-6S, ΔdiHS-6S; HS-diS, disulfated unsaturated disaccharides of HS; HS-TriS, trisulfated unsaturated disaccharides of HS.

PANC1 cells are exposed to the external environment. Mucin-type glycans of BxPC3 cells were obviously different from those of PANC1 cells. Core 2 structure was the major glycan in BxPC3 cells, and its modified structures (i.e., polylactosaminyl structure and fucosylated glycans) were also observed in BxPC3 cells. Mare and Trinchera reported that BxPC3 cells expressed polylactosamine-type glycans [46]. The profiles of GAGs of PANC1 cells are quite interesting, and only HA and low-sulfated HS (HS0S) were observed. HA and HS were also the major GAGs in BxPC3 cells (moderately differentiated pancreatic cancer cell lines), and profiles similar to those of PANC1 cells were reported. The expression level of HA was increased in pancreatic cancer cells [35], and its increase was a risk factor for tumor proliferation and metastasis [36,47]. In addition, BxPC3 cells obviously expressed CS, which was not observed in PANC1 cells. Sulfated mucin-type glycans were characteristically observed in colon cancer cell lines, HCT15 and LS174T. HCT15 cells expressed core 2 and polylactosamine-type glycans as the major mucin-type glycans. In addition, sialyl-T and disialyl-T were abundant in HCT15 cells. Most of the abundant mucin-type glycans in LS174T cells were fucosylated. LS174T cells also expressed large amounts of Tn antigen and polylactosamine-type glycans. This is a specific feature of LS174T cells in which both truncated and extended glycans were present. Both HCT15 and LS174T cells contained low-sulfated HS (HS0S) as the major GAGs. In contrast, the level of HS sulfation in HCT15 cells was a little bit higher than that observed in LS174T cells. However, relative abundance of ΔdiCS-6S in LS174T cells was higher than that in HCT15 cells. We previously reported that the profiles of mucin-type glycans were dramatically changed with differentiation stages of gastric cancer cell lines [38]. Poorly differentiated gastric cancer cells (MKN45 cells) expressed large amounts of extended polylactosamine-type glycans with molecular masses greater than 6000 [38]. In addition, trisialylated mucin-type glycans were characteristically observed in MKN45 cells. In contrast, polylactosamine-type glycans were not observed in well-differentiated gastric cancer cells (MKN7 cells). In MKN7 cells, glycans of core 2 structure were observed abundantly. This means that elongation of core 2 structure to polylactosamine-type glycan is suppressed in MKN7 cells, although further studies on the related synthetic enzymes are required. Profiles of GAGs in these two gastric cancer cells were quite different. HA and low-sulfated HS (HS0S) were abundant, but CSs were scarcely observed in MKN45 cells. In contrast, CSs were the major GAGs in MKN7 cells. Relative abundance of ΔdiCS-4S was especially distinct in MKN7 cells.

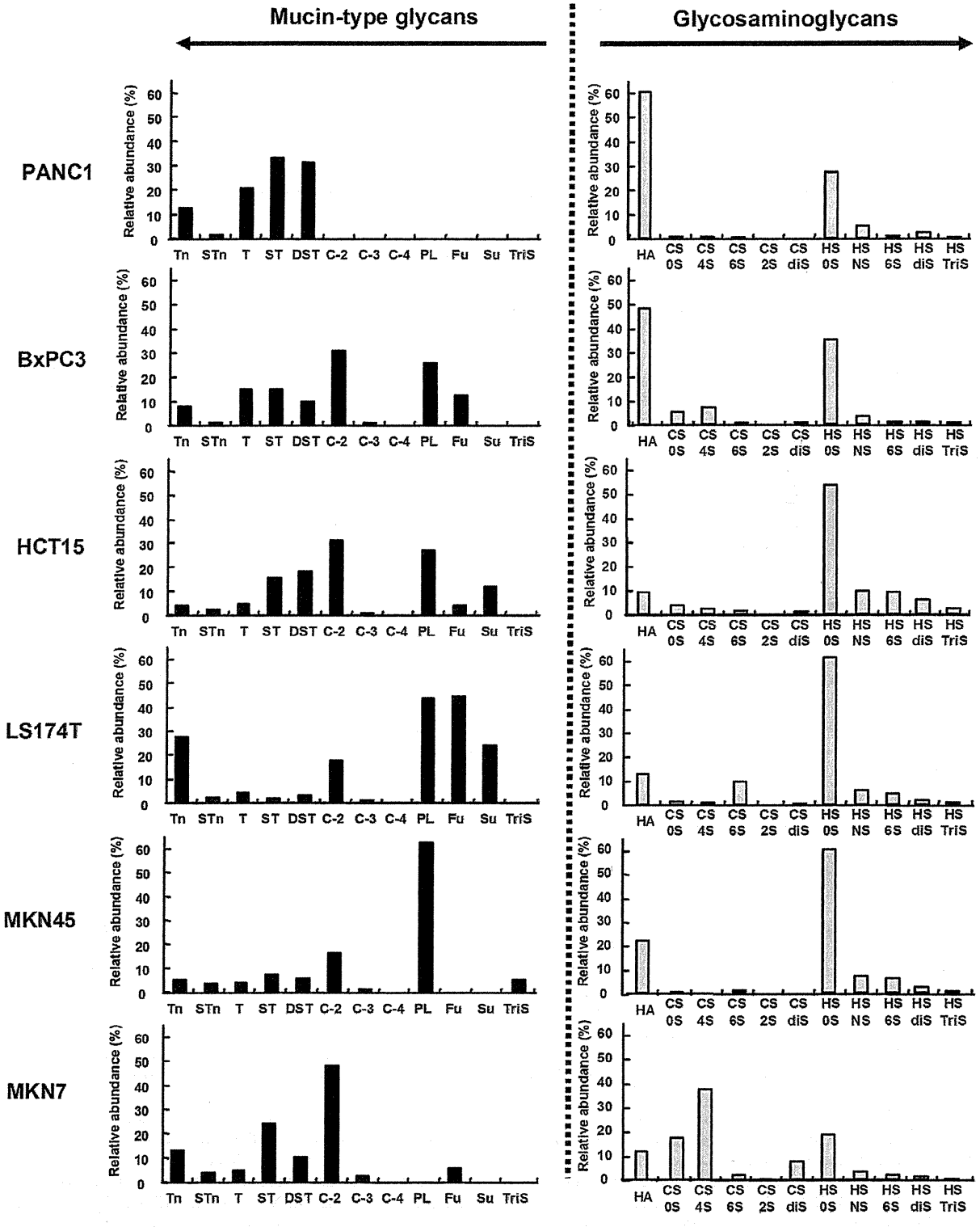

Fig.8. Characterization of six epithelial cancer cell lines. The contents of mucin-type glycans and GAGs are displayed as black bars and gray bars, respectively. Calculation of relative abundances and abbreviations are the same as in Fig. 7.

Although further studies are required, these results may indicate that GAGs play an important role in differentiation of gastric cancer cells.

As described above, it was revealed that our methods are useful to characterize the various cancer cell lines. In the future, we will apply these methods to compare *O*-glycan profiles between cancer